8-2020

Greening-Induced Runoff Loss in the Western United States

Xueyan Zhang
Utah State University

GREENING-INDUCED RUNOFF LOSS IN THE WESTERN UNITED STATES

by

Xueyan Zhang

A thesis submitted in partial fulfillment
of the requirements of the degree

of

MASTER OF SCIENCE

in

Watershed Science

Approved:

_____	_____
Jiming Jin, Ph.D.	Patrick Belmont, Ph.D.
Major Professor	Committee Member
_____	_____
David Stevens, Ph.D.	Janis L. Boettinger, Ph.D.
Committee Member	Acting Vice Provost of Graduate Studies

UTAH STATE UNIVERSITY
Logan, Utah

2020

ABSTRACT

Greening-Induced Runoff Loss in the Western United States

by

Xueyan Zhang, Master of Science

Utah State University, 2020

Major Professor: Dr. Jiming Jin
Department: Watershed Sciences

Water resources across the western United States (western US) are projected to decrease in the future. Previous studies have assessed future runoff changes across the western US, but vegetation physiology has not been properly represented in these studies. To better understand runoff changes during 2016–2099 across the western US, I selected the community Noah land surface model with multiparameterization options (Noah-MP) coupled with improved dynamic vegetation root processes because of its capability to reproduce historical (1981–2015) regional runoff variability and trends. Noah-MP was driven by high-resolution (~12 km) and statistically downscaled outputs of three global climate models (GFDL-ESM2G, IPSL-CM5A-MR, and MIROC5) under the Representative Concentration Pathway (RCP) 4.5 and 8.5 scenarios. Based on trend and multiple linear regression analysis, leaf area index contributed most to transpiration increases across the western US. Transpiration significantly increased during spring and summer because of intense water demands by vegetation. Therefore, runoff remarkably declined across five regions (Upper and Lower Colorado, Great Basin, Pacific Northwest,

and California), especially during summer. Annual runoff was reduced by up to -79%, -100%, -70%, -16%, and -35% in these five regions, respectively. In addition, the magnitude of runoff reduction was generally larger under RCP 8.5 than under RCP 4.5 due to higher transpiration. Overall, this study provides reliable fine-scale projections of water resources and clarifies that vegetation could reduce future water availability for the western US.

(69 pages)

PUBLIC ABSTRACT

Greening-induced runoff loss in the western United States

Xueyan Zhang

This study assessed how vegetation will influence long-term runoff trends across the western United States (western US) in the future. I used a land surface model with improved dynamic vegetation root processes to better quantify regional runoff trends across five regions (Upper and Lower Colorado, Great Basin, Pacific Northwest, and California). The model was driven by statistically downscaled and bias-corrected outputs from three global climate models under the Representative Concentration Pathway 4.5 and 8.5 scenarios. Vegetation greening dominated significant transpiration increases that contributed most to increasing evapotranspiration across the western US, especially during spring and summer. Consistent with these trends, runoff exhibited drastic reductions over these five regions, especially during summer. Annual runoff was reduced by up to -79%, -100%, -71%, -16%, and -35% across these regions, respectively. Overall, this study provides reliable fine-scale future projections of water resources for the western US and suggests that vegetation will aggravate the water crisis the western US is currently facing.

DEDICATION

This manuscript is dedicated to my family.

ACKNOWLEDGMENTS

I would like to express deepest thanks to my adviser Dr. Jiming Jin, who brought me into the world of hydrology and gave me constant support. He taught me how to pursue science and think critically, although he is always busy. From the bottom of my heart, I am grateful to be his student, to learn from him, and to have the opportunities he gave me. Without him, I would not have come so far. I would also like to thank my committee members Dr. Patrick Belmont and Dr. David Stevens for giving me valuable comments on my thesis. Thanks also go to Dr. Guo-yue Niu at the University of Arizona for providing me the model used in this project, as well as leaf area index data and valuable suggestions during my analysis. I am thankful to people in my lab for their generous help during my graduate study, especially to Zeyu Zhou and Xiaogang Ma for giving me suggestions on my draft, and to Yajun Si for helping me with the data downscaling and draft. I also want to thank Kendall Becker in the Wildland Resources Department for her help through my thesis writing. Her passion about science writing motivates me to work hard on writing and guides me in my scientific writing. Finally, I would like to thank my friends for their encouragement during these years.

This work was partially supported by the Department of Watershed Sciences.

Xueyan Zhang

CONTENTS

Page

LIST OF TABLES

Table Page

LIST OF FIGURES

CHAPTER 1

INTRODUCTION

Increasing temperatures, changing precipitation patterns, and elevated atmospheric carbon dioxide (CO_2) are occurring in the western United States (western US) due to climate change. Annual temperature in the western US has risen over 0.8 °C since 1901 (Vose et al. 2017), and annual precipitation has decreased in parts of the western US (Easterling et al. 2017). These changes have resulted in snowpack loss (McCabe and Wolock 2009; Mote et al. 2005; Pierce et al. 2008), evapotranspiration (ET) increases (Hamlet et al. 2007; Walter et al. 2004), streamflow timing shifts (Clow 2010), and runoff reductions (Forbes et al. 2018) in the western US. Meanwhile, elevated CO_2 and climate change have caused remarkably increased vegetation (Zhu et al. 2017) that can also affect runoff through transpiration. Given climate change impacts on water resources in the already dry western US, reliable future projections of water availability at fine spatial scales are required.

Previous studies have projected runoff declines across the western US in response to future climate change (Ficklin et al. 2013; Hamlet and Lettenmaier 1999; Jung and Chang 2011; Mankin et al. 2017; Mankin et al. 2019; Naz et al. 2016; Sun et al. 2016; Yang et al. 2019). However, some issues remain in current studies. First, a coarse model resolution (typically 100–250 km) cannot reflect realistic vegetation distributions, leading to inaccurate vegetation influences on runoff. Additionally, coarse resolutions cannot provide useful regional hydrological information for water resource planning and management (Naz et al. 2016; Sun et al. 2016). Second, most studies have evaluated runoff changes between historical and future periods of ~30 years. However, if selected

periods are influenced by internal multidecadal climate variations, their results could provide less confidence in projected runoff changes (Jung and Chang 2011). Third, vegetation dynamics are not adequate in current models. Most process-based models fail to consider plant water storage or dynamic root processes, leading to lower ecosystem resilience and transpiration. Additionally, soil water stress, instead of plant water stress, is parameterized to account for water limitations on stomatal closure and photosynthesis, which cannot reflect vegetation buffering impacts on transpiration and photosynthesis. Neglect of vegetation physiology can result in misrepresentations of transpiration and further runoff in the future (Mankin et al. 2017; Sun et al. 2016). Therefore, it is important to represent mechanistic vegetation processes with high-resolution modeling at long-term scales.

The goal of this study was to better understand vegetation responses to climate change and its influences on runoff in the western US in the 21st century. This was achieved by projecting leaf area index (LAI), transpiration, ET, and runoff under the Representative Concentration Pathway (RCP) 4.5 and 8.5 scenarios, using the recently improved community Noah land surface model with multiparameterization options (Noah-MP). I aimed mainly to (1) quantify vegetation changes for the future western US, represented by LAI; and (2) project the impacts of vegetation transpiration on runoff across the western US using high-resolution modeling.

CHAPTER 2

METHODOLOGY

2.1 Study region

The semi-arid western US was selected as my study area. The elevation of the western US ranges from below sea level in coastal regions to over 4,000 m in the Southern Rockies (Fig. 1). Mean annual temperature ranges from ~2 °C in the Southern Rockies to over 20 °C in Death Valley. Mean annual precipitation is high in mountain ranges, with the most precipitation, over 2,000 mm, in the Pacific Northwest. Most precipitation in the western US falls as snow from October through April (Kapnick et al. 2018). Major vegetation types include shrubland, grassland, and forest, covering over 80% of the western US.

2.2 Model

This study was conducted using Noah-MP, a widely used land surface model that can simulate exchanges of water, carbon, and energy in the terrestrial ecosystem (Cai et al. 2014a; Cai et al. 2014b; Ma et al. 2017; Niu et al. 2011; Pilotto et al. 2015; Wang et al. 2018; Yang et al. 2011). The model is an advanced version of the Noah model and provides multiple combinations of physical parameterizations (Niu et al. 2011). The model structure includes one canopy layer, four soil layers with a total depth of 2 m, up to three snow layers depending on the snow depth, and an unconfined aquifer layer (Niu et al. 2011). Noah-MP represents surface heterogeneity with a “semi-tile” scheme that separately computes the longwave radiation and heat fluxes for vegetated and bare

fractions of a grid cell (Niu et al. 2011). Details about the major physical processes involved in this study are given below.

Noah-MP incorporates a simple but efficient dynamic vegetation model (Niu et al. 2011). This model considers photosynthesis, respiration, turnover, carbon allocation, and leaf death due to cold temperatures and water stress, accounting for vegetation types (Dickinson et al. 1998; Niu et al. 2011; Parton et al. 1978). It is worth noting that the vegetation type distribution is constant in Noah-MP. It separately calculates the photosynthesis of sunlit and shaded leaves. The gross photosynthesis rate is calculated as the minimum of three limiting rates: the light-limited rate, the Rubisco-limited rate, and the limitation by the transport of photosynthate for C3 plants (Ma et al. 2017; Niu et al. 2011). The gross photosynthesis rate is likely reduced due to stomatal closure when plant water stress occurs. Here, plant water stress is parameterized by available, minimum, and maximum plant water storage related to plant dry mass. Consequently, Noah-MP allocates more photosynthetically fixed carbon to roots (Parton et al. 1978), and thus roots can extract more soil water to meet transpiration demands. Root water uptake rate is determined by root surface area, soil water potential, and transpiration pull (Schymanski et al. 2008; Wang et al. 2018). Roots cannot extract water from soil when soil water potential is below the wilting point (~-30 bar), and therefore only plant water storage can supply transpiration demand. Taken together, vegetation carbon and water cycles interact with each other through dynamic root processes.

Noah-MP introduces a TOPMODEL-based runoff scheme to compute saturated-excess surface and subsurface runoff (Niu et al. 2011). Noah-MP also considers the contribution of impermeable area to surface runoff. Subsurface runoff is related to the

depth of the groundwater table and the topographic index. Vegetation directly affects runoff amount through transpiration. Collectively, energy, water, and carbon cycles are linked by mechanistic vegetation processes in Noah-MP.

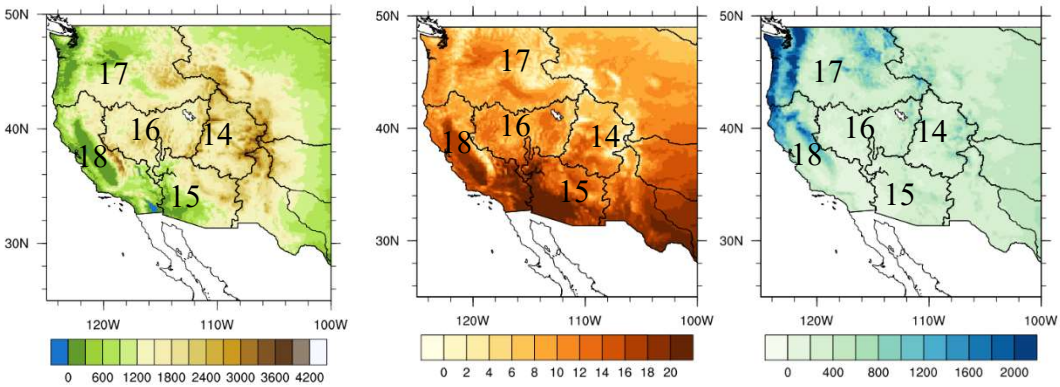

FIG. 1. (Left) elevation (unit: m), (center) average annual temperature (unit: °C), and (right) average annual precipitation (unit: mm) across the western US. The thicker black boundaries represent two-digit hydrologic units (HUC2): 14: Upper Colorado, 15: Lower Colorado, 16: Great Basin, 17: Pacific Northwest, and 18: California.

2.3 Data

2.3.1 Historical atmospheric data

Phase 2 of the North American Land Data Assimilation System (NLDAS-2; Xia et al. 2012) atmospheric forcing data were used to drive Noah-MP. This dataset spans from January 1979 to the present at a resolution of 0.125° with an hourly time step throughout North America. It provides the atmospheric variables required by Noah-MP, including downward shortwave and longwave radiation fluxes, surface air pressure and temperature, specific humidity, wind speed, and precipitation rate. The atmospheric variables, except precipitation, were generated by the 3-hourly and 32-km North American Regional Reanalysis through spatiotemporal interpolation and vertical adjustment (Cosgrove et al. 2003). The precipitation field of NLDAS-2 was derived by

disaggregating unified daily gauge-only precipitation analysis from the Climate Prediction Center with weights from other datasets based on availability, such as radar (Xia et al. 2012). Additionally, this dataset has been widely verified and employed in modeling studies for the United States (Cai et al. 2014b; Ma et al. 2017; Xia et al. 2012).

2.3.2 Future atmospheric data

The Fifth Phase of the Coupled Model Intercomparison Project data (Taylor et al. 2012) were used as the forcing input into Noah-MP for future projections. Nonlinear yearly CO_2 concentration (Prather et al. 2013) was used to represent future CO_2 changes. The outputs of three long-term global climate model (GCM) experiments (Table 3) were selected because they provide all atmospheric variables required by Noah-MP. These three models represent divergent intensities of future climate change, where the most aggressive increase in air temperature occurs in IPSL-CM5A-MR (Buotte et al. 2019), and the least temperature increase in GFDL-ESM2G. Precipitation generally exhibited insignificant seasonal and annual changes across most of the western US, except for significant year-round precipitation decreases over the Upper and Lower Colorado for the IPSL-CM5A-MR model under RCP 8.5 (Table A3TABLE A3). However, the coarse resolution of these data (~150–250 km) could fail to capture accurate surface heterogeneity and climates compared to high-resolution data. Therefore, I first downscaled these 3-hourly data, except precipitation, to the resolution of NLDAS-2 (0.125°) using bilinear interpolation. Second, the downscaled data were statistically bias-corrected by keeping the probability distributions of historical values similar to those of NLDAS-2 through linear regression models (Dettinger et al. 2004). Three-hourly precipitation was created using daily downscaled precipitation data (Abatzoglou 2013)

for these selected GCMs with the method described by Buotte et al. (2019) and then interpolated to 0.125° by bilinear interpolation. Through downscaling and bias-corrections, the biases in these GCM outputs were reduced for the historical period (Fig. 2; Fig. A1; Table 1), making the future projections more reliable.

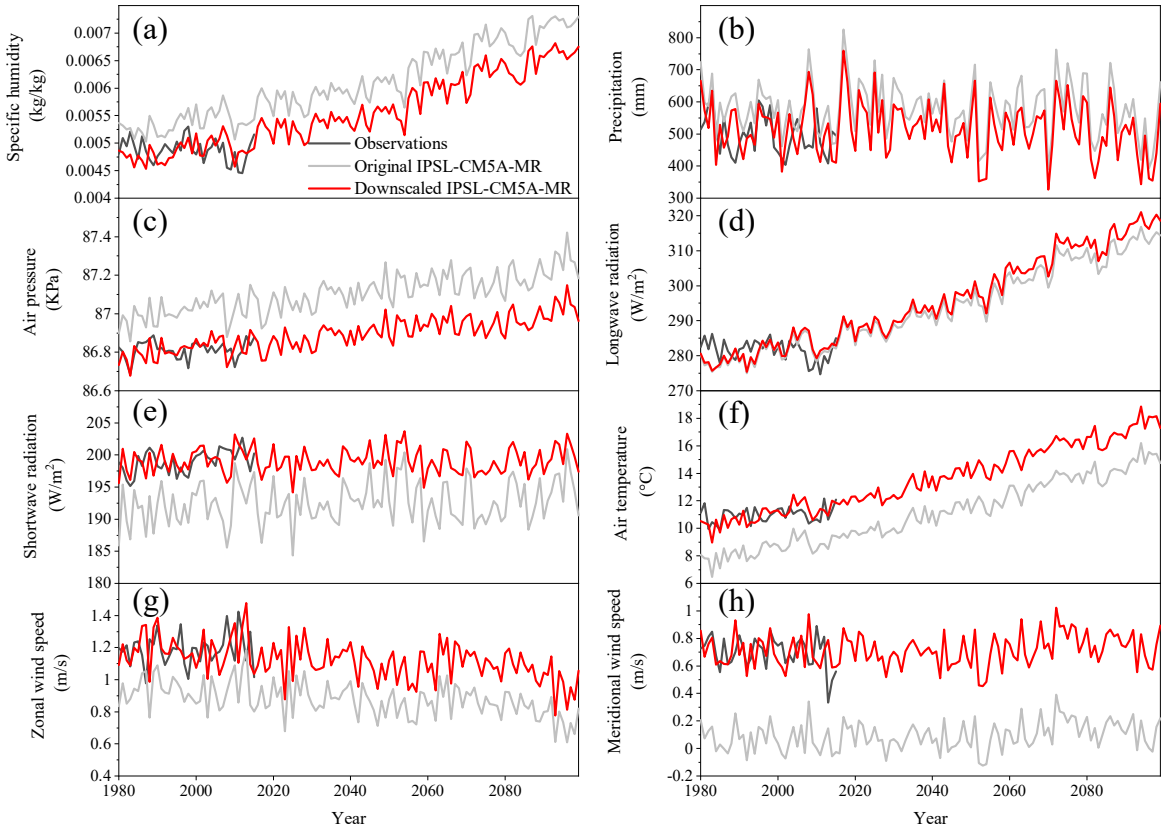

FIG. 2. Annual (a) specific humidity at 2 m (kg/kg), (b) total precipitation (mm), (c) surface air pressure (kPa), (d) downward longwave radiation (W/m^2), (e) downward shortwave radiation (W/m^2), (f) air temperature at 2 m (°C), (g) zonal wind speed at 10 m (m/s), and (h) vertical wind speed at 10 m (m/s) of observations (black line), original IPSL-CM5A-MR RCP 8.5 (gray line), and downscaled IPSL-CM5A-MR RCP 8.5 (red line) averaged over the western US during 1980–2099.

2.3.3 Leaf area index data

The improved Moderate Resolution Imaging Spectroradiometer (MODIS) LAI (Yuan et al. 2011) during 2002–2015 was selected to evaluate simulated LAI. This

improved product has been widely used in land surface and climate modeling due to its high spatiotemporal resolution and accuracy (Boisier et al. 2014; Fan et al. 2015; Ke et al. 2012; Wei et al. 2017). It has a spatial resolution of 1 km and a temporal resolution of 8 days. MODIS LAI was interpolated into the resolution of NLDAS-2 (0.125°) and aggregated into a monthly product.

2.3.4 Evapotranspiration data

ET from the FLUXNET Model Tree ensemble (FLUXNET-MTE; Jung et al. 2011) was used to assess the performance of Noah-MP in simulating ET. This dataset was generated by upscaling water, CO_2, and energy fluxes measured at FLUXNET sites, which are densely located in the United States, and incorporating remote sensing, meteorological, and land cover data through a machine learning approach (Jung et al. 2011; Ma et al. 2017). This dataset has been extensively used to evaluate ET simulated by land surface models (Cai et al. 2014b; Ma et al. 2017). FLUXNET-MTE spans from 1982 through 2011, with a spatial resolution of 0.5° and a temporal resolution of 1 month. This dataset was downscaled to the resolution of NLDAS-2 by bilinear interpolation.

2.3.5 Runoff data

USGS WaterWatch monthly runoff data were used for model validation. This runoff dataset was generated using stream gage observations, the corresponding drainage basins, and HUC boundaries (Brakebill et al. 2011; Ma et al. 2017). USGS WaterWatch data have been applied to evaluate modelled runoff (Cai et al. 2014a; Cai et al. 2014b; Ma et al. 2017) and investigate runoff changes (Clow 2010; Sagarika et al. 2014). The

monthly runoff averaged for each five regions (Fig. 1) during 1981–2015 were used in simulated runoff validation.

2.4 Experimental design

2.4.1 Model evaluation

I first ran Noah-MP with NLDAS-2 of 1980 seventy times to allow the model to reach an equilibrium that could act as an initial condition (Liang et al. 2019). Then, the historical simulation was conducted from 1981 through 2015 with the initial condition and driven by NLDAS-2. For parameterization schemes, most options (Table 2) were the same as those in Ma et al. (2017) because they represent all previous augmentations in Noah-MP (Ma et al. 2017). Recent improvements in precipitation partitioning based on wet-bulb temperature (Wang et al. 2019) and dynamic root processes were also used in this study. To quantify the performance of Noah-MP in simulating LAI, ET, and runoff, I calculated the spatial distribution of the difference, RMSE, and Pearson Correlation coefficient (r) between simulations and observations using the MODIS, FLUXNET-MTE, and USGS WaterWatch runoff datasets across the western US, respectively.

2.4.2 Future projections

The future projections from 2016 through 2099 were performed with the downscaled and bias-corrected forcing data (Table 3). The parameterization schemes were the same as in the historical simulation. The initial condition was created by a 70-year simulation of 2015 using future atmospheric forcing data. RCPs 4.5 and 8.5 were selected because they represent intermediate and high emission scenarios (Li et al. 2017), respectively. I calculated linear trends of LAI, transpiration, ET, and runoff during 2016–

2099 and examined the significance of these trends using the Mann-Kendall test. Here, ET consists of transpiration, evaporation, and sublimation.

To figure out the relationships between climatic variables and vegetation physiological controls and projected seasonal transpiration changes, multiple linear regression (MLR) was used with five explanatory variables: precipitation, temperature, solar radiation, CO_2, and LAI. Each variable's contribution to seasonal transpiration trends is the product of their regression coefficients derived from MLR and linear regression trends. Stepwise regression was used to remove insignificant predictors.

TABLE 1. Root mean square error (RMSE) of annual specific humidity (huss), precipitation (pr), surface air pressure (ps), longwave radiation (rlds), shortwave radiation (rsds), air temperature (tas), zonal wind speed (uas), and vertical wind speed (vas) averaged over the western US between original (Org), downscaled (Down), and NLDAS-2 during 1980–2015 for GFDL-ESM2G, IPSL-CM5A-MR , and MIROC5 (from left to right) under RCPs 4.5 and 8.5. Here, the unit of huss is 10^{-3} kg/kg, and units of other variables are the same as in Figure 2.

Scenario	RCP 4.5						RCP 8.5					
Variable	Org	Down	Org	Down	Org	Down	Org	Down	Org	Down	Org	Down
huss	0.6	0.3	0.6	0.3	1.0	0. 4	0.5	0.3	0.6	0.3	1.0	0.4
pr	275.2	92.5	120.3	91.8	218.4	93.0	262.6	86.3	116.2	94.0	228.6	95.3
ps	161.9	60.4	216.0	56.4	79.2	70.4	161.5	61.7	213.5	61.3	78.3	71.1
rlds	9.1	4.8	5.0	5.1	10.9	6.0	8.35	4.1	4.7	4.7	10.6	5.8
rsds	4.5	2.6	8.0	2.2	10.3	2.3	4.3	2.4	7.8	2.4	10.6	2.8
tas	3.7	0.8	2.6	0.8	0.9	1.0	3.7	0.8	2.6	0.8	0.7	0.8
uas	0.5	0.2	0.3	0.2	0.4	0.2	0.5	0.2	0.3	0.2	0.4	0.2
vas	0.5	0.1	0.7	0.1	0.5	0.2	0.5	0.1	0.7	0.2	0.5	0.2

TABLE 2. Parameterization options used in this study.

Physical process parameterizations	Selected option
Dynamic vegetation	2. On
Stomatal resistance	1. Ball-Berry
Soil moisture factor controlling stomatal resistance	1. Noah
Runoff and groundwater	1. TOPMODEL with groundwater
Surface exchange coefficient for heat	1. M-O
Supercooled liquid water in frozen soil	1. No iteration
Frozen soil permeability	1. Linear effects
Radiation transfer	1. Modified two-stream
Snow surface albedo	2. CLASS
Precipitation partitioning	4. Wet-bulb temperature
Snow/soil temperature time scheme	1. Semi-implicit
Dynamic root	1. On

TABLE 3. Models used in this study and their spatial resolutions.

Model	Source	Spatial resolution
GFDL-ESM2G	Geophysical Fluid Dynamics Laboratory, USA	2.5°×2.0°
IPSL-CM5A-MR	Institute Pierre-Simon Laplace MR: Medium resolution, France	2.5°×1.3°
MIROC5	Atmosphere and Ocean Research Institute (The University of Tokyo), National Institute for Environmental Studies, and Japan Agency for Marine-Earth Science and Technology, Japan	1.4°×1.4°

CHAPTER 3

RESULTS

3.1 Model validation

Simulated LAI, ET, and runoff from Noah-MP were evaluated with available observations across spatiotemporal scales to ensure that future projections of these variables would be reliable. Modelled spatiotemporal distributions of LAI reflected those of observations (Fig. A2). LAI was largely underestimated in the coastal regions and Cascades because parameters related to vegetation photosynthesis, respiration, and leaf dying and turnover were not calibrated well. Monthly time series of simulated LAI exhibited a low RMSE of less than 0.3 m^2/m^2 and a high r of over 0.82 (Fig. 3), despite a slight time lag that is likely due to limited vegetation process representation in Noah-MP. Overall, Noah-MP generally simulated LAI distributions and magnitudes well.

Noah-MP also produced similar spatial patterns of seasonal total ET compared with FLUXNET-MTE (Fig. A3). The spatial distribution of simulated ET was similar to that of annual precipitation where high values appeared mainly on the west coast and in mountain ranges (Fig. 1). The negative bias of ET over the west coast, Cascades, and Sierra Nevada during spring and summer may be due to underestimated transpiration from low LAI (Fig. A2). Furthermore, monthly simulated ET averaged over each of regions 14–18 matched observations well, featuring a low RMSE of less than 7.1 mm/month and a high r of above 0.84 (Fig. 4). mm/month and a high r of above 0.84 (Fig. 4).

Simulated monthly runoff over regions 14–18 captured the magnitude and variation of USGS WaterWatch monthly runoff, with an RMSE of less than 11

mm/month and an r of higher than 0.82 (Fig. 5). The Pacific Northwest and California have greater simulated and observed annual runoff compared with other regions because of higher precipitation (Fig. 1). In addition, both simulated and observed annual regional runoff exhibited reductions, with the largest declines in California. The good performance of simulated annual runoff trends gave me confidence in runoff projections (Fig. 6). In summary, the overall agreement between simulations and observations indicated that Noah-MP was capable of projecting LAI, ET, and runoff for the western US.

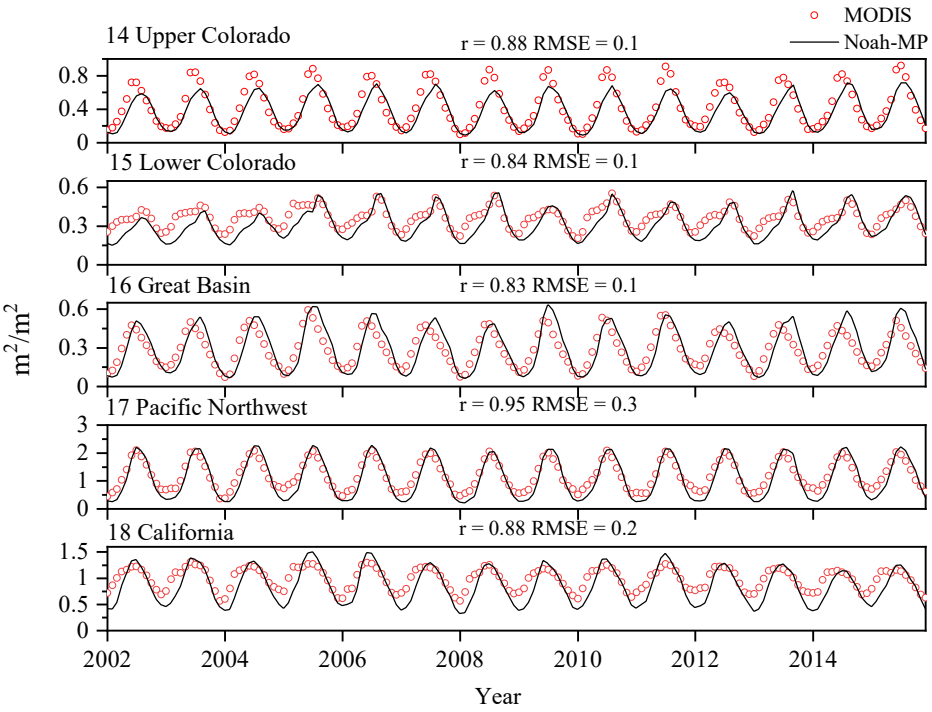

FIG. 3. Monthly LAI of MODIS (red circles) and Noah-MP (black line) over HUC2 regions from 2002 through 2015 (unit: m^2/m^2).

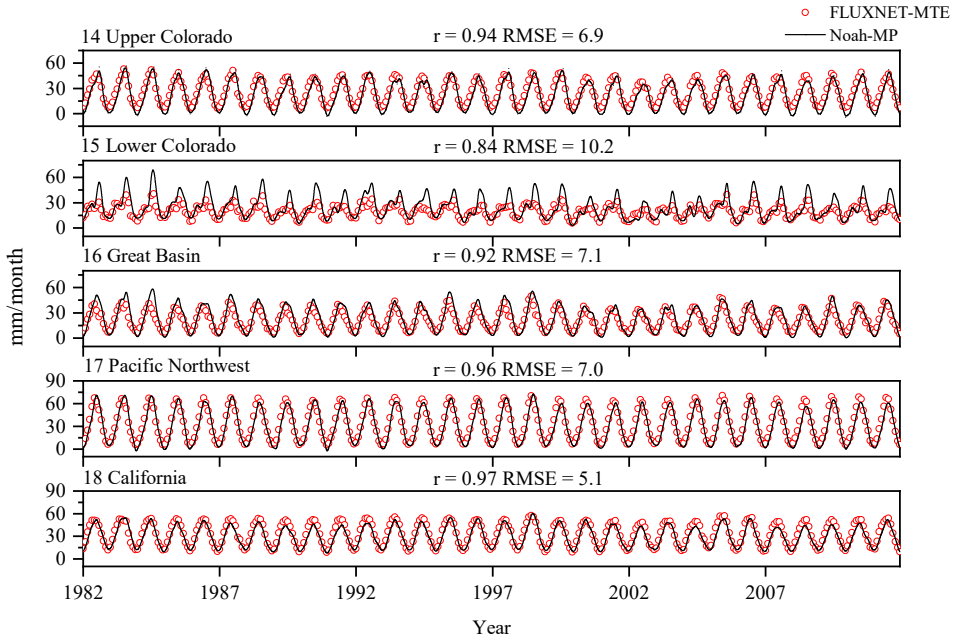

FIG. 4. Monthly ET of FLUXNET-MTE (red circles) and Noah-MP (black line) over HUC2 regions from 1982 through 2011 (unit: mm/month).

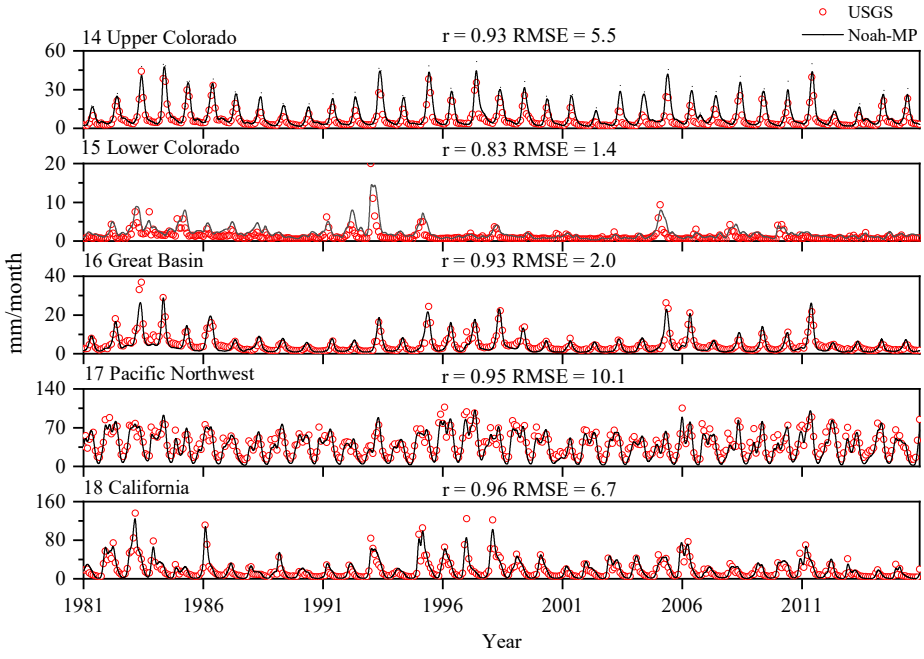

FIG. 5. Monthly runoff of USGS (red circles) and Noah-MP (black line) over HUC2 regions during 1981–2015 (unit: mm/month).

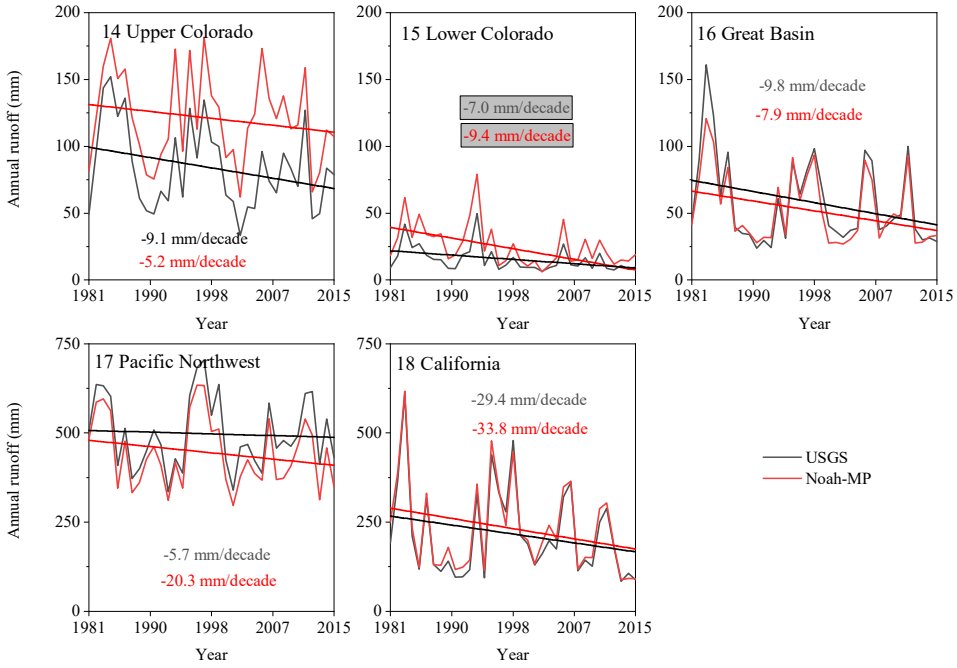

FIG. 6. Time series of annual runoff of USGS (black line) and Noah-MP (red line) over HUC2 regions during 1981–2015 (unit: mm) with their trends (unit: mm/decade). The numbers with gray background are significant ($p < 0.05$).

3.2 Future projections

3.2.1 Vegetation changes

From 2016 through 2099, seasonal mean LAI across the western US exhibited robust increasing trends, especially during spring and summer (Fig 7). Models largely agreed on spatial patterns of seasonal LAI trends and showed higher LAI increases under RCP 8.5 than under RCP 4.5. Interestingly, the GFDL-ESM2G model generally exhibited larger increasing trends than the other two models, which was likely due to less intense temperature increases. The most notable LAI increases occurred in mountain ranges, such as the Southern Rockies and Sierra Nevada, but there were smaller increases in lowland regions. Spring, summer, fall, and winter mean LAI trends over regions 14–18 reached

0.15, 0.21, 0.08, and 0.03 m^2/m^2/decade, respectively (Table A1). Summer mean LAI trends for each region were the largest compared with other seasons.

3.2.2 Impact of vegetation changes on transpiration

Transpiration was projected to significantly increase across the western US during 2016 through 2099 (Fig. 8). Models showed good agreement on overall spatial patterns of seasonal total transpiration trends. Models generally produced larger transpiration increases under RCP 8.5 than under RCP 4.5. Like spatial distributions of seasonal LAI trends, large transpiration increases appeared in mountain ranges, such as the Sierra Nevada and Southern Rockies. Spring and summer transpiration greatly increased, with regional averages of up to 8 mm/decade because of high water consumption by vegetation, but with no significant change during winter due to low temperature (Table A2). Fall transpiration averaged over each region showed less agreement on the direction of change among models. On an annual basis, regions 14–18 exhibited large transpiration increases of up to 124%, 86%, 140%, 50%, and 32%, respectively. Furthermore, transpiration followed similar spatiotemporal patterns as ET (Fig. A4) and contributed most to annual ET increases in the future (Fig. A5).

Contributions of vegetation and climatic factors to seasonal transpiration trends for each region were computed by MLR as described in the methodology. Results show that LAI contributed most to increasing transpiration trends, except in a few regions where the influence of temperature exceeded that of LAI (Fig. 9; Fig. 10; Fig. 11). Interestingly, rising temperature increased transpiration over all regions and seasons through the opening of stomata and higher vapor pressure deficits. Rising CO_2 generally resulted in transpiration decreases through the closing of stomata (Kirschbaum and

McMillan 2018). Because the negative impacts of CO_2 exceeded the positive impacts of other variables, transpiration over the Lower Colorado during summer for IPSL-CM5A-MR and MIROC5 significantly declined. In addition, RCP 8.5, the high CO_2 emission scenario, reduced transpiration more than RCP 4.5. Solar radiation and precipitation played a minor role in transpiration changes partially due to their slight changes (Table A3; Table A4). Overall, vegetation greening, represented by LAI, dominated significant transpiration and ET increases in the future.

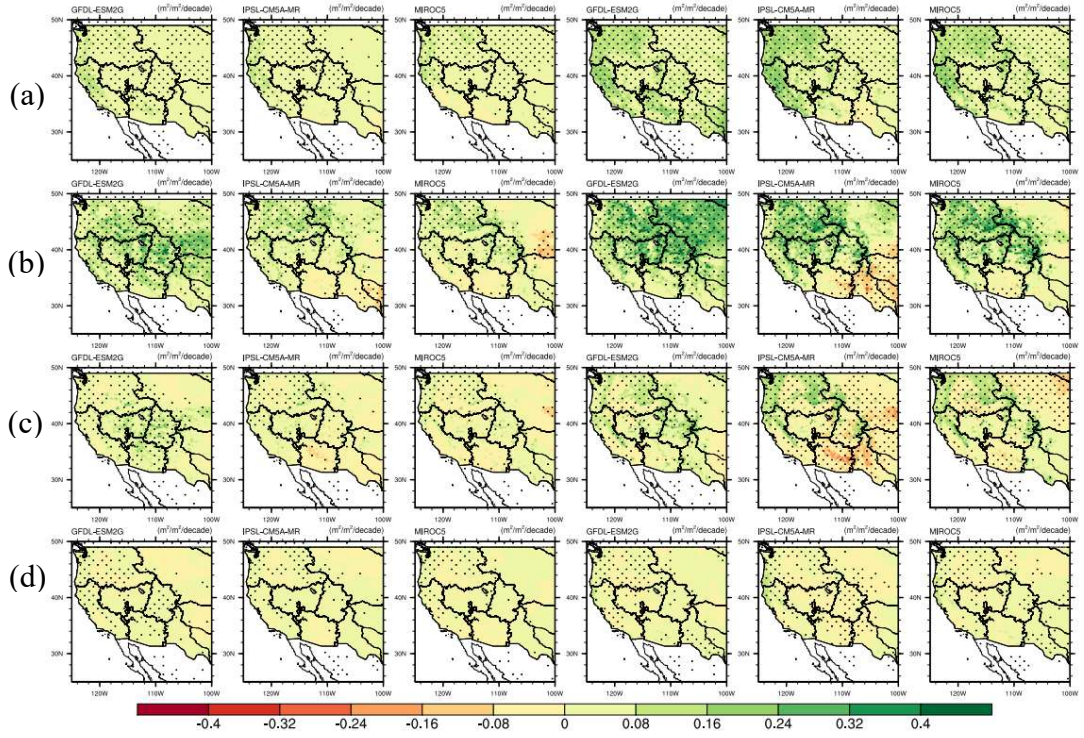

FIG. 7. Spatial distribution of trends in (a) spring, (b) summer, (c) fall, and (d) winter mean LAI during 2016–2099 (unit: m^2/m^2/decade) under RCPs 4.5 (left three columns) and 8.5 (right three columns). Stippling indicates regions with statistically significant trends ($p < 0.05$).

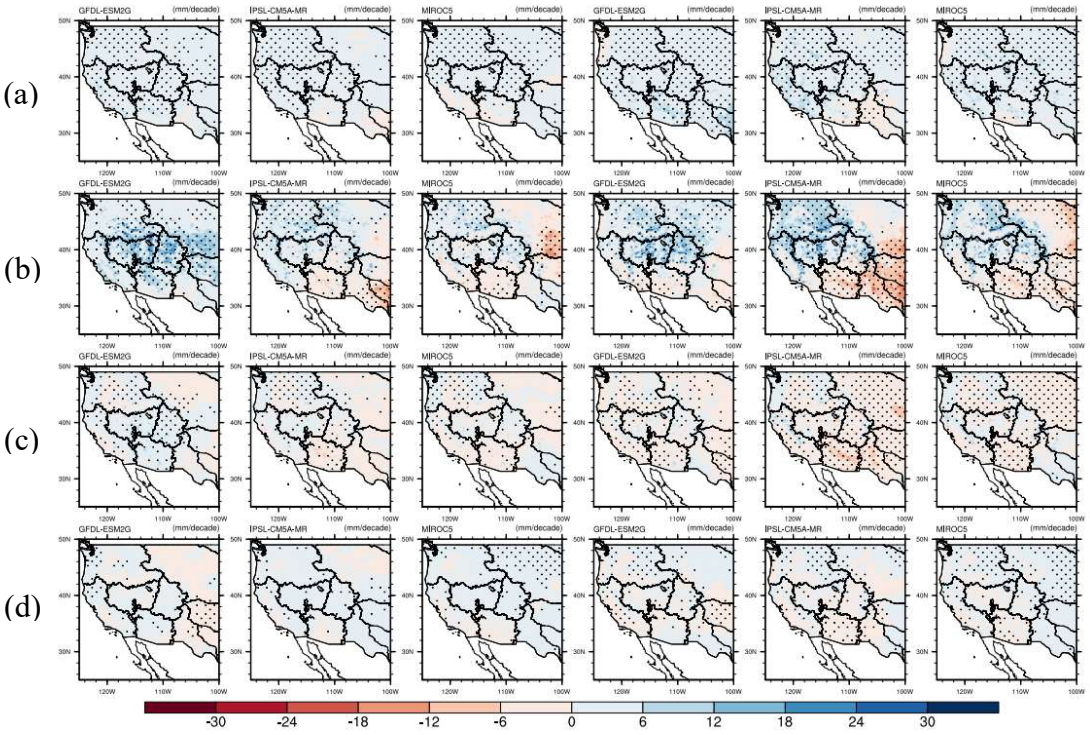

FIG. 8. Same as in Figure 7, but for total transpiration.

3.2.3 Impact of vegetation changes on runoff

Runoff declined remarkably across the western US in the future despite model and regional differences. All models exhibited consistency in substantial summer runoff reductions except the Upper Colorado for the GFDL-ESM2G model under RCP 4.5. Fall runoff averaged over the Upper and Lower Colorado and Great Basin declined among almost all models, while there was less agreement among models over the Pacific Northwest and California. In addition, spring runoff changes for most regions were less certain in all cases. Interestingly, year-round runoff was reduced over the Lower Colorado. Overall, annual runoff averaged over regions 14–18 was reduced by up to -79% (-15 mm/decade), -100% (-4 mm/decade), -71% (-7 mm/decade), -16% (-10 mm/decade), and -35% (-14 mm/decade), respectively.

Vegetation directly influences runoff generation through transpiration. Summer runoff reductions were caused mainly by vegetation because summer precipitation in most cases exhibited insignificant changes (Table A3). There is one exception, where declining summer runoff over the Lower Colorado for the GFDL-ESM2G and MIROC5 models was likely due to less precipitation (Table A3), even though there were transpiration decreases (Table A2). For spring and fall runoff, increasing transpiration resulted in less runoff, despite low consistency in runoff changes among all cases. Given insignificant precipitation changes (Table A3) and significant transpiration increases (Table A2) at an annual scale, annual runoff reductions were controlled largely by vegetation. However, decreased annual runoff over the Lower Colorado for the IPSL-CM5A-MR and MIROC5 models likely resulted from less precipitation.

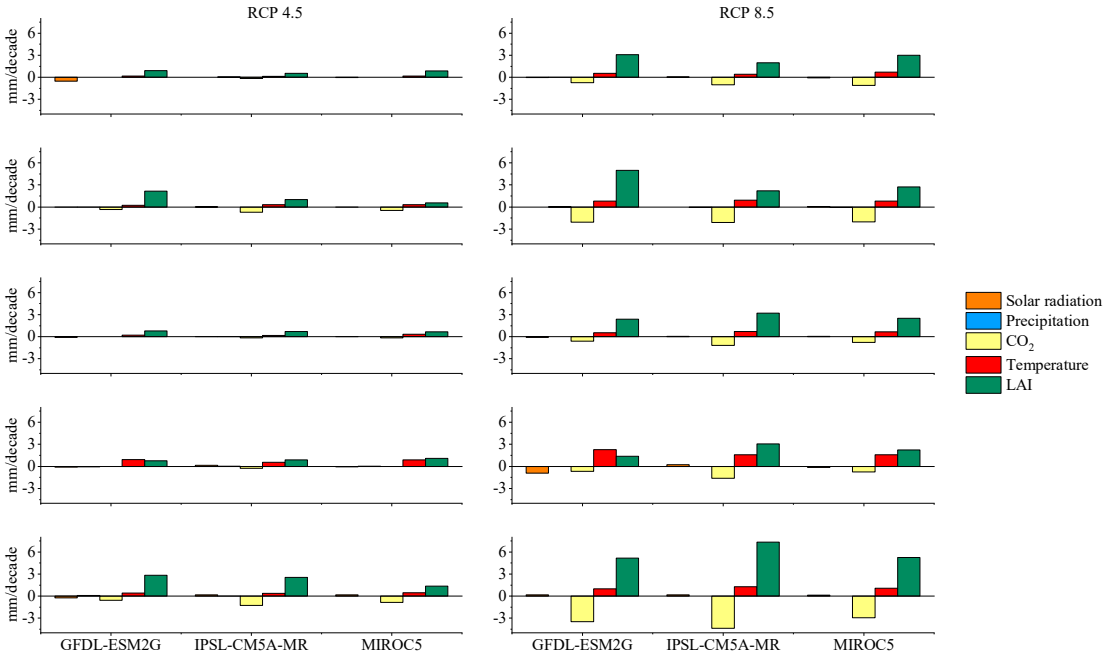

FIG. 9. Solar radiation (orange), precipitation (blue), CO_2 (yellow), temperature (red), and LAI (green) contributions to transpiration trends during spring for regions 14 (top) – 18 (bottom) for three GCMs under RCPs 4.5 and 8.5.

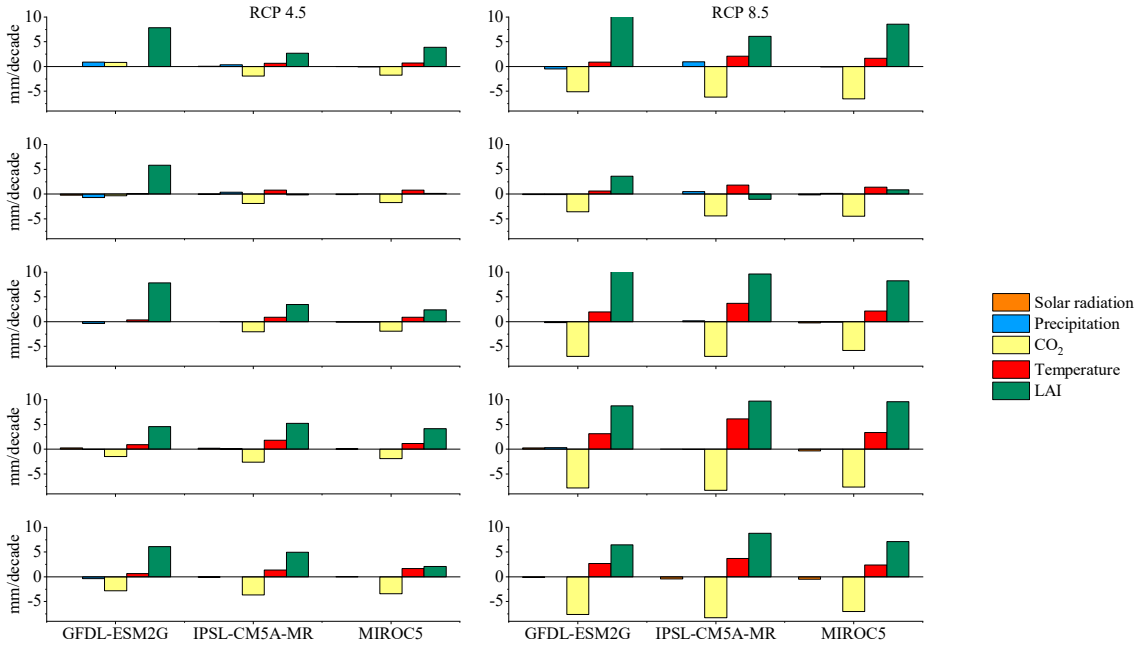

FIG. 10. Same as in Figure 9, but for summer.

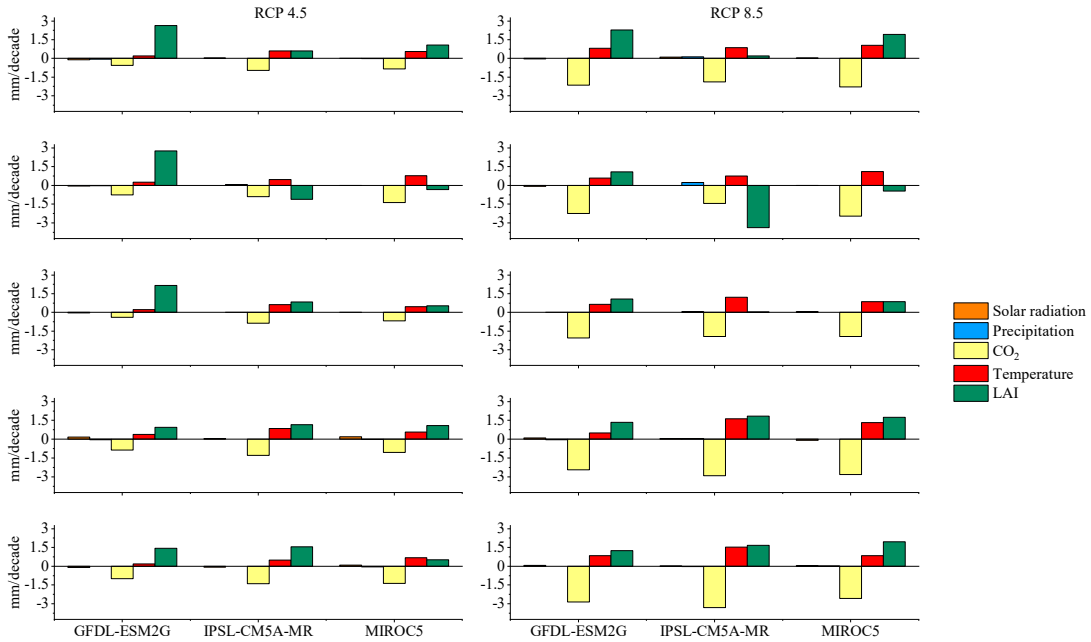

FIG. 11. Same as in Figure 9, but for fall.

TABLE 4. Seasonal and annual runoff trends averaged over regions 14–18 (unit: mm/decade). Significant trends are shown in bold ($p < 0.05$).

Scenario		RCP 4.5			RCP 8.5		
Model		GFDL-ESM2G	IPSL-CM5A-MR	MIROC5	GFDL-ESM2G	IPSL-CM5A-MR	MIROC5
Region 14	Spring	**3**	**-1**	1	**3**	**-3**	0
	Summer	1	**-4**	**-3**	**-4**	**-8**	**-6**
	Fall	1	**-1**	**-1**	**-1**	**-3**	**-1**
	Winter	0	**-1**	**0**	**0**	**-1**	**-1**
	Annual	**4**	**-7**	**-3**	-2	**-15**	**-8**
Region 15	Spring	0	**-1**	**-1**	**-1**	**-1**	**-1**
	Summer	0	**0**	**0**	**0**	**-1**	**0**
	Fall	0	**-1**	**0**	**0**	**-1**	**0**
	Winter	0	**-1**	**-1**	**0**	**-1**	**-1**
	Annual	-1	**-3**	**-2**	**-2**	**-4**	**-2**
Region 16	Spring	0	-1	**-2**	**-2**	**-3**	**-2**
	Summer	-1	**-2**	**-2**	**-2**	**-3**	**-2**
	Fall	0	**0**	**0**	**0**	**-1**	**0**
	Winter	0	0	**0**	**0**	**0**	**0**
	Annual	0	**-3**	**-4**	**-5**	**-7**	**-5**
Region 17	Spring	2	2	1	3	**-6**	0
	Summer	**-6**	**-5**	**-7**	**-7**	**-6**	**-6**
	Fall	**-2**	1	0	-2	1	**-2**
	Winter	-1	**5**	2	4	2	5
	Annual	-7	4	-4	-2	**-10**	**-2**
Region 18	Spring	1	1	-3	**-5**	-4	-2
	Summer	-1	-1	**-3**	**-3**	**-3**	**-2**
	Fall	0	1	**-1**	**-1**	**0**	**0**
	Winter	-3	6	-6	-6	-2	2
	Annual	-2	8	**-13**	**-14**	-9	**-2**

CHAPTER 4

DISCUSSION

4.1 Driving factors of future vegetation changes

Projected vegetation greening in the western US from this study was similar to previous studies (Mahowald et al. 2016; Mankin et al. 2017; Mankin et al. 2019). To explore the driving factors in vegetation greening, I conducted an additional experiment with constant CO_2 of 2016 and detrended temperatures. LAI increasing trends were largely reduced in this additional experiment (Fig. A6), suggesting that elevated CO_2 and rising temperatures contribute most to vegetation greening. However, other factors may also influence vegetation greening, such as changing precipitation (Mahowald et al. 2016) and increasing specific humidity. For example, significant declining summer precipitation over the Lower Colorado for the IPSL-CM5A-MR model (Table A3) likely results in vegetation water stress and thus reduces LAI. Rising specific humidity (Fig. 2a) could reduce transpiration by lowering atmospheric evaporative demands and thus increase LAI to some extent.

4.2 Future runoff changes and vegetation influences on these changes

Projected runoff reductions across the western US in this study were generally consistent with other studies (Mankin et al. 2019; Naz et al. 2016; Udall and Overpeck 2017). However, disagreement on the direction of runoff change for some regions still exists due to downscaling, modeling, evaluation metrics, and forcing inputs (Naz et al. 2016). For example, Naz et al. (2016) reported increased year-round runoff over the Lower Colorado in the near future (2011–2050) compared with a historical period (1966–

2005), which is the opposite of this study, likely because Naz et al. (2016) used the median changes from ten models.

Based on the water balance equation (P-ET-R=δS) at an annual scale, runoff trends are influenced by precipitation, ET, and water storage change. The mean annual water storage anomaly was near zero, indicating that precipitation was partitioned into ET and runoff at long-term scales (Bonan 2015). Because annual precipitation exhibited insignificant changes in most regions, LAI-dominated ET increases clearly significantly reduced annual runoff in the future. However, absolute trends of ET and runoff did not always match, suggesting that insignificant precipitation and water storage change could still influence runoff trends to some extent.

At seasonal scales, vegetation does not account for the full picture of runoff changes. For example, earlier spring snowmelt due to warming likely enhances spring runoff but reduces summer runoff. This can also partially explain why models exhibited high consistency in summer runoff reductions but not for spring runoff changes. Groundwater discharge during dry seasons may ameliorate runoff loss. Atmospheric evaporative demand varies with the season and leads to changing vegetation water consumption. Therefore, snowpack, groundwater, and climatic factors such as temperature need to be investigated in future studies.

4.3 Model limitations

Like all studies, this study has some limitations. First, Noah-MP does not consider any nitrogen cycles or nitrogen limitations on vegetation photosynthesis. The lack of nitrogen representation could lead to overestimations of CO_2 uptake (Tharammal et al. 2019), LAI (Mahowald et al. 2016; Mankin et al. 2017), and transpiration.

Second, the vegetation types and distribution were kept constant in this study. However, natural disturbances could result in tree mortality and then shifting vegetation types. Bark beetle outbreaks and wildfire have resulted in tree mortality in nearly 15% of the forested area across the western US during the past three decades (Hicke et al. 2016). Tree mortality is also projected to likely increase in the future across the western US, especially in the Southwest (Buotte et al. 2019; Jiang et al. 2013; Thorne et al. 2018). Jiang et al. (2013) projected that half of regions dominated by evergreen needles in the western US will shift into shrub- and grass-dominant types by the end of the 21st century under the future A2 emission scenario. These potential vegetation changes may increase, not change, or reduce runoff amount by altering the hydrologic cycle (Goeking and Tarboton 2020). Although the forested area comprises less than 20% of the western US, future work is needed to better understand these natural disturbances' impacts on future water resources.

4.4 Uncertainties

Two major sources of uncertainties include lack of transpiration observations and limited understanding of vegetation physiological processes. First, because large-scale transpiration observations are not available (Lawrence et al. 2007), I evaluated Noah-MP's performance in simulating ET with FLUXNET-MTE. Although simulated ET performed well, the accuracy of ET partitioning into transpiration and evaporation is still unknown. This also hinder us from calibrating Noah-MP's simulated transpiration for the whole region. Second, despite the improved dynamic vegetation root processes in Noah-MP, our current understanding of vegetation dynamics is still limited, such as

competition and succession, especially in a changing climate. To reduce these uncertainties, large-scale observations and field experiments are required.

Uncertainties also exist in the model evaluation process from validation datasets. The MODIS LAI product is mainly generated through MODIS reflectance data, a look-up table, and a three-dimensional radiation transfer model (Yan et al. 2016). If this main algorithm fails, the alternate algorithm is used to calculate LAI based on the relationship between LAI and Normalized Difference Vegetation Index. Uncertainties of the observed LAI tend to be high in some cases, such as dense canopy and complex terrain. Therefore, it can explain why relatively higher LAI bias in coastal regions and the Cascades partially due to larger uncertainties of LAI observations. Moreover, the water balance for some grid cells may be not closed because of different sources of validation datasets and their uncertainties (Cai et al. 2014b). That is why the Lower Colorado exhibited runoff and ET overestimations together.

Despite the good performance of linear regression models in bias correcting CMIP5 data, there are still some problems related to this method. First, reduced interannual variabilities for some variables occur (Fig. 2). Second, statistical methods usually neglect dynamic atmospheric processes (Xue et al. 2014), compared to dynamic downscaling. Therefore, our downscaling method could be improved to account for these problems for future work.

Overall, this study provides a reliable assessment of runoff changes by representing dynamic vegetation root processes. This work can therefore help water resource planning and management for the western US. Given the importance of vegetation in water resources, future work should better investigate how vegetation will

respond and adapt to climate change, and how it will impact water resources such as runoff and groundwater.

CHAPTER 5

CONCLUSION

This study investigated how vegetation will influence runoff in the future across the western US. To examine this, a mechanistic Noah-MP model coupled with dynamic vegetation root processes was driven by high-resolution, statistically downscaled climate data from three GCMs under RCPs 4.5 and 8.5. First, I analyzed LAI and transpiration trends for regions 14–18 and used MLR to assess climatic and vegetation contributions to transpiration trends. Second, I evaluated seasonal and annual regional runoff trends and analyzed vegetation influences on those trends. Through trend analysis, two main findings resulted from this study:

(1) Transpiration contributed most to future ET increases across the western US. Vegetation greening controlled transpiration increases in most cases, followed by temperature. Elevated CO_2 reduced transpiration and even resulted in declining trends in transpiration during summer and fall in some regions. Precipitation and solar radiation contributed the least to transpiration changes. Annual transpiration increased remarkably, mainly during spring and summer when water is most required for vegetation growth.

(2) Consistent with LAI-induced transpiration increases, runoff reductions occurred over regions 14–18, especially during summer, suggesting severe water shortages across the western US in the future. Taken together, increased vegetation growth aggravates the water crisis that already exists in the western US.

REFERENCES

Abatzoglou, J. T., 2013: Development of gridded surface meteorological data for ecological applications and modelling. *Int. J. Climatol.*, **33,** 121-131, https://doi.org/10.1002/joc.3413.

Boisier, J., N. de Noblet-Ducoudré, and P. Ciais, 2014: Historical land-use induced evapotranspiration changes estimated from present-day observations and reconstructed land-cover maps. *Hydrol. Earth Syst. Sci.*, **11**, https://doi.org/10.5194/hess-18-3571-2014.

Bonan, G., 2015: *Ecological climatology: concepts and applications.* Cambridge University Press, https://doi.org/10.1017/CBO9781107339200.

Brakebill, J. W., D. M. Wolock, and S. Terziotti, 2011: Digital Hydrologic Networks Supporting Applications Related to Spatially Referenced Regression Modeling 1. *J. Amer. Water Resour. Assoc.*, **47,** 916-932, https://doi.org/10.1111/j.1752-1688.2011.00578.x.

Buotte, P. C., S. Levis, B. E. Law, T. W. Hudiburg, D. E. Rupp, and J. J. Kent, 2019: Near‐future forest vulnerability to drought and fire varies across the western United States. *Glob. Chang. Biol.*, **25,** 290-303, https://doi.org/10.1111/gcb.14490.

Cai, X., Z. L. Yang, C. H. David, G. Y. Niu, and M. Rodell, 2014a: Hydrological evaluation of the Noah‐MP land surface model for the Mississippi River Basin. *J. Geophys. Res. Atmos.*, **119,** 23-38, https://doi.org/10.1002/2013JD020792.

Cai, X., Z. L. Yang, Y. Xia, M. Huang, H. Wei, L. R. Leung, and M. B. Ek, 2014b: Assessment of simulated water balance from Noah, Noah‐MP, CLM, and VIC over CONUS using the NLDAS test bed. *J. Geophys. Res. Atmos.*, **119,** 13,751-713,770, https://doi.org/10.1002/2014JD022113.

Clow, D. W., 2010: Changes in the timing of snowmelt and streamflow in Colorado: a response to recent warming. *J. Climate*, **23,** 2293-2306, https://doi.org/10.1175/2009JCLI2951.1.

Cosgrove, B. A., and Coauthors, 2003: Real‐time and retrospective forcing in the North American Land Data Assimilation System (NLDAS) project. *J. Geophys. Res. Atmos.*, **108**, https://doi.org/10.1029/2002JD003118.

Dettinger, M. D., D. R. Cayan, M. K. Meyer, and A. E. Jeton, 2004: Simulated hydrologic responses to climate variations and change in the Merced, Carson, and American River basins, Sierra Nevada, California, 1900–2099. *Climatic Change*, **62,** 283-317, https://doi.org/10.1023/B:CLIM.0000013683.13346.4f.

Dickinson, R. E., M. Shaikh, R. Bryant, and L. Graumlich, 1998: Interactive canopies for a climate model. *J. Climate*, **11,** 2823-2836, https://doi.org/10.1175/1520-0442(1998)011<2823:ICFACM>2.0.CO;2.

Easterling, D. R., and Coauthors, 2017: Precipitation change in the United States, http://doi.org/10.7930/J0H993CC.

Fan, X., Z. Ma, Q. Yang, Y. Han, R. Mahmood, and Z. Zheng, 2015: Land use/land cover changes and regional climate over the Loess Plateau during 2001–2009. Part I: observational evidence. *Climatic Change*, **129,** 427-440, http://doi.org/10.1007/s10584-014-1068-5.

Ficklin, D. L., I. T. Stewart, and E. P. Maurer, 2013: Climate change impacts on streamflow and subbasin-scale hydrology in the Upper Colorado River Basin. *PLoS One*, **8,** e71297, https://doi.org/10.1371/journal.pone.0071297.

Forbes, W. L., and Coauthors, 2018: Contribution of environmental forcings to US runoff changes for the period 1950–2010. *Environ. Res. Lett.*, **13,** 054023, https://doi.org/10.1088/1748-9326/aabb41.

Goeking, S. A., and D. G. Tarboton, 2020: Forests and water yield: A synthesis of disturbance effects on streamflow and snowpack in western coniferous forests. *J. For.*, **118,** 172-192, https://doi.org/10.1093/jofore/fvz069.

Hamlet, A. F., and D. P. Lettenmaier, 1999: Effects of climate change on hydrology and water resources in the Columbia River Basin 1. *J. Amer. Water Resour. Assoc.*, **35,** 1597-1623, https://doi.org/10.1111/j.1752-1688.1999.tb04240.x.

Hamlet, A. F., P. W. Mote, M. P. Clark, and D. P. Lettenmaier, 2007: Twentieth-century trends in runoff, evapotranspiration, and soil moisture in the western United States. *J. Climate*, **20,** 1468-1486, https://doi.org/10.1175/JCLI4051.1.

Hicke, J. A., A. J. Meddens, and C. A. Kolden, 2016: Recent tree mortality in the western United States from bark beetles and forest fires. *For. Sci.*, **62,** 141-153, https://doi.org/10.5849/forsci.15-086.

Jiang, X., and Coauthors, 2013: Projected future changes in vegetation in western North America in the twenty-first century. *J. Climate*, **26,** 3671-3687, https://doi.org/10.1175/JCLI-D-12-00430.1.

Jung, I. W., and H. Chang, 2011: Assessment of future runoff trends under multiple climate change scenarios in the Willamette River Basin, Oregon, USA. *Hydrol. Processes*, **25,** 258-277, https://doi.org/10.1002/hyp.7842.

Jung, M., and Coauthors, 2011: Global patterns of land‐atmosphere fluxes of carbon dioxide, latent heat, and sensible heat derived from eddy covariance, satellite, and

meteorological observations. *J. Geophys. Res. Biogeosci.*, **116**, https://doi.org/10.1029/2010JG001566.

Kapnick, S. B., and Coauthors, 2018: Potential for western US seasonal snowpack prediction. *Proc. Natl. Acad. Sci.*, **115,** 1180-1185, https://doi.org/10.1073/pnas.1716760115.

Ke, Y., L. Leung, M. Huang, A. M. Coleman, H. Li, and M. S. Wigmosta, 2012: Development of high resolution land surface parameters for the Community Land Model. *Geosci. Model Dev.*, **5,** 1341, https://doi.org/10.5194/gmd-5-1341-2012.

Kirschbaum, M. U., and A. M. McMillan, 2018: Warming and Elevated CO 2 Have Opposing Influences on Transpiration. Which is more Important? *Curr. For. Rep.*, **4,** 51-71, https://doi.org/10.1007/s40725-018-0073-8.

Lawrence, D. M., P. E. Thornton, K. W. Oleson, and G. B. Bonan, 2007: The partitioning of evapotranspiration into transpiration, soil evaporation, and canopy evaporation in a GCM: Impacts on land–atmosphere interaction. *J. Hydrometeor.*, **8,** 862-880, https://doi.org/10.1175/JHM596.1.

Li, D., M. L. Wrzesien, M. Durand, J. Adam, and D. P. Lettenmaier, 2017: How much runoff originates as snow in the western United States, and how will that change in the future? *Geophys. Res. Lett.*, **44,** 6163-6172, https://doi.org/10.1002/2017GL073551.

Liang, J., Z. Yang, and P. Lin, 2019: Systematic Hydrological Evaluation of the Noah-MP Land Surface Model over China. *Adv. Atmos. Sci.*, **36,** 1171-1187, https://doi.org/10.1007/s00376-019-9016-y.

Ma, N., G. Y. Niu, Y. Xia, X. Cai, Y. Zhang, Y. Ma, and Y. Fang, 2017: A systematic evaluation of Noah‐MP in simulating land‐atmosphere energy, water, and carbon exchanges over the continental United States. *J. Geophys. Res. Atmos.*, **122,** 12,245-212,268, https://doi.org/10.1002/2017JD027597.

Mahowald, N., F. Lo, Y. Zheng, L. Harrison, C. Funk, D. Lombardozzi, and C. Goodale, 2016: Projections of leaf area index in earth system models. *Earth Syst. Dyn.*, **7**, https://doi.org/10.5194/esd-7-211-2016.

Mankin, J. S., J. E. Smerdon, B. I. Cook, A. P. Williams, and R. Seager, 2017: The curious case of projected twenty-first-century drying but greening in the American West. *J. Climate*, **30,** 8689-8710, https://doi.org/10.1175/JCLI-D-17-0213.1.

Mankin, J. S., R. Seager, J. E. Smerdon, B. I. Cook, and A. P. Williams, 2019: Mid-latitude freshwater availability reduced by projected vegetation responses to climate change. *Nat. Geosci.*, **12,** 983-988, https://doi.org/10.1038/s41561-019-0480-x.

McCabe, G. J., and D. M. Wolock, 2009: Recent declines in western US snowpack in the context of twentieth-century climate variability. *Earth Interact.*, **13,** 1-15, https://doi.org/10.1175/2009EI283.1.

Mote, P. W., A. F. Hamlet, M. P. Clark, and D. P. Lettenmaier, 2005: Declining mountain snowpack in western North America. *Bull. Amer. Meteor. Soc.*, **86,** 39-50, https://doi.org/10.1175/BAMS-86-1-39.

Naz, B. S., S.-C. Kao, M. Ashfaq, D. Rastogi, R. Mei, and L. C. Bowling, 2016: Regional hydrologic response to climate change in the conterminous United States using high-resolution hydroclimate simulations. *Global Planet. Change*, **143,** 100-117, https://doi.org/10.1016/j.gloplacha.2016.06.003.

Niu, G. Y., and Coauthors, 2011: The community Noah land surface model with multiparameterization options (Noah‐MP): 1. Model description and evaluation with local‐scale measurements. *J. Geophys. Res. Atmos.*, **116**, https://doi.org/10.1029/2010JD015139.

Parton, W., J. Singh, and D. Coleman, 1978: A model of production and turnover of roots in shortgrass prairie. *J. Appl. Ecol.***,** 515-541, https://doi.org/10.2307/2402608.

Pierce, D. W., and Coauthors, 2008: Attribution of declining western US snowpack to human effects. *J. Climate*, **21,** 6425-6444, https://doi.org/10.1175/2008JCLI2405.1.

Pilotto, I. L., D. A. Rodríguez, J. Tomasella, G. Sampaio, and S. C. Chou, 2015: Comparisons of the Noah-MP land surface model simulations with measurements of forest and crop sites in Amazonia. *Meteorol. Atmospheric Phys.*, **127,** 711-723, https://doi.org/10.1007/s00703-015-0399-8.

Prather, M., G. Flato, P. Friedlingstein, C. Jones, J. Lamarque, H. Liao, and P. Rasch, 2013: Annex II: Climate system scenario tables. *Climate change***,** 1395-1445,

Sagarika, S., A. Kalra, and S. Ahmad, 2014: Evaluating the effect of persistence on long-term trends and analyzing step changes in streamflows of the continental United States. *J. Hydrol.*, **517,** 36-53, https://doi.org/10.1016/j.jhydrol.2014.05.002.

Schymanski, S. J., M. Sivapalan, M. L. Roderick, J. Beringer, and L. B. Hutley, 2008: An optimality-based model of the coupled soil moisture and root dynamics. *Hydrol. Earth Syst. Sci.*, **12,** 913-932, https://doi.org/10.5194/hess-12-913-2008.

Sun, S., G. Sun, E. C. Mack, S. McNulty, P. V. Caldwell, K. Duan, and Y. Zhang, 2016: Projecting water yield and ecosystem productivity across the United States by linking an ecohydrological model to WRF dynamically downscaled climate data. *Hydrol. Earth Syst. Sci.*, **20,** 935-952, https://doi.org/10.5194/hess-20-935-2016.

Taylor, K. E., R. J. Stouffer, and G. A. Meehl, 2012: An overview of CMIP5 and the experiment design. *Bull. Amer. Meteor. Soc.*, **93,** 485-498, https://doi.org/10.1175/BAMS-D-11-00094.1.

Tharammal, T., G. Bala, D. Narayanappa, and R. Nemani, 2019: Potential roles of CO 2 fertilization, nitrogen deposition, climate change, and land use and land cover change on the global terrestrial carbon uptake in the twenty-first century. *Climate Dyn.*, **52,** 4393-4406, https://doi.org/10.1007/s00382-018-4388-8.

Thorne, J. H., H. Choe, P. A. Stine, J. C. Chambers, A. Holguin, A. C. Kerr, and M. W. Schwartz, 2018: Climate change vulnerability assessment of forests in the Southwest USA. *Climatic Change*, **148,** 387-402, https://doi.org/10.1007/s10584-017-2010-4.

Udall, B., and J. Overpeck, 2017: The twenty‐first century Colorado River hot drought and implications for the future. *Water Resour. Res.*, **53,** 2404-2418, https://doi.org/10.1002/2016WR019638.

Vose, R., D. R. Easterling, K. Kunkel, and M. Wehner, 2017: Temperature changes in the United States, http://doi.org/10.7930/J0N29V45.

Walter, M. T., D. S. Wilks, J.-Y. Parlange, and R. L. Schneider, 2004: Increasing evapotranspiration from the conterminous United States. *J. Hydrometeor.*, **5,** 405-408, https://doi.org/10.1175/1525-7541(2004)005<0405:IEFTCU>2.0.CO;2.

Wang, P., and Coauthors, 2018: Implementing dynamic root optimization in Noah‐MP for simulating phreatophytic root water uptake. *Water Resour. Res.*, **54,** 1560-1575, https://doi.org/10.1002/2017WR021061.

Wang, Y. H., P. Broxton, Y. Fang, A. Behrangi, M. Barlage, X. Zeng, and G. Y. Niu, 2019: A Wet‐Bulb Temperature‐Based Rain‐Snow Partitioning Scheme Improves Snowpack Prediction Over the Drier Western United States. *Geophys. Res. Lett.*, **46,** 13825-13835, https://doi.org/10.1029/2019GL085722.

Wei, Z., K. Yoshimura, L. Wang, D. G. Miralles, S. Jasechko, and X. Lee, 2017: Revisiting the contribution of transpiration to global terrestrial evapotranspiration. *Geophys. Res. Lett.*, **44,** 2792-2801, https://doi.org/10.1002/2016GL072235.

Xia, Y., and Coauthors, 2012: Continental‐scale water and energy flux analysis and validation for the North American Land Data Assimilation System project phase 2 (NLDAS‐2): 1. Intercomparison and application of model products. *J. Geophys. Res. Atmos.*, **117**, https://doi.org/10.1029/2011JD016048.

Xue, Y., Z. Janjic, J. Dudhia, R. Vasic, and F. De Sales, 2014: A review on regional dynamical downscaling in intraseasonal to seasonal simulation/prediction and major

factors that affect downscaling ability. *Atmos. Res.*, **147,** 68-85, https://doi.org/10.1016/j.atmosres.2014.05.001.

Yan, K., and Coauthors, 2016: Evaluation of MODIS LAI/FPAR product collection 6. Part 2: Validation and intercomparison. *Remote Sens.*, **8,** 460, https://doi.org/10.3390/rs8060460.

Yang, Y., M. L. Roderick, S. Zhang, T. R. McVicar, and R. J. Donohue, 2019: Hydrologic implications of vegetation response to elevated CO_2 in climate projections. *Nat. Climate Change*, **9,** 44-48, https://doi.org/10.1038/s41558-018-0361-0.

Yang, Z. L., and Coauthors, 2011: The community Noah land surface model with multiparameterization options (Noah‐MP): 2. Evaluation over global river basins. *J. Geophys. Res. Atmos.*, **116**, https://doi.org/10.1029/2010JD015139.

Yuan, H., Y. Dai, Z. Xiao, D. Ji, and W. Shangguan, 2011: Reprocessing the MODIS Leaf Area Index products for land surface and climate modelling. *Remote Sens. Environ.*, **115,** 1171-1187, https://doi.org/10.1016/j.rse.2011.01.001.

Zhu, Z., S. Piao, X. Lian, R. B. Myneni, S. Peng, and H. Yang, 2017: Attribution of seasonal leaf area index trends in the northern latitudes with “optimally” integrated ecosystem models. *Glob. Chang. Biol.*, **23,** 4798-4813, https://doi.org/10.1111/gcb.13723.

APPENDICES

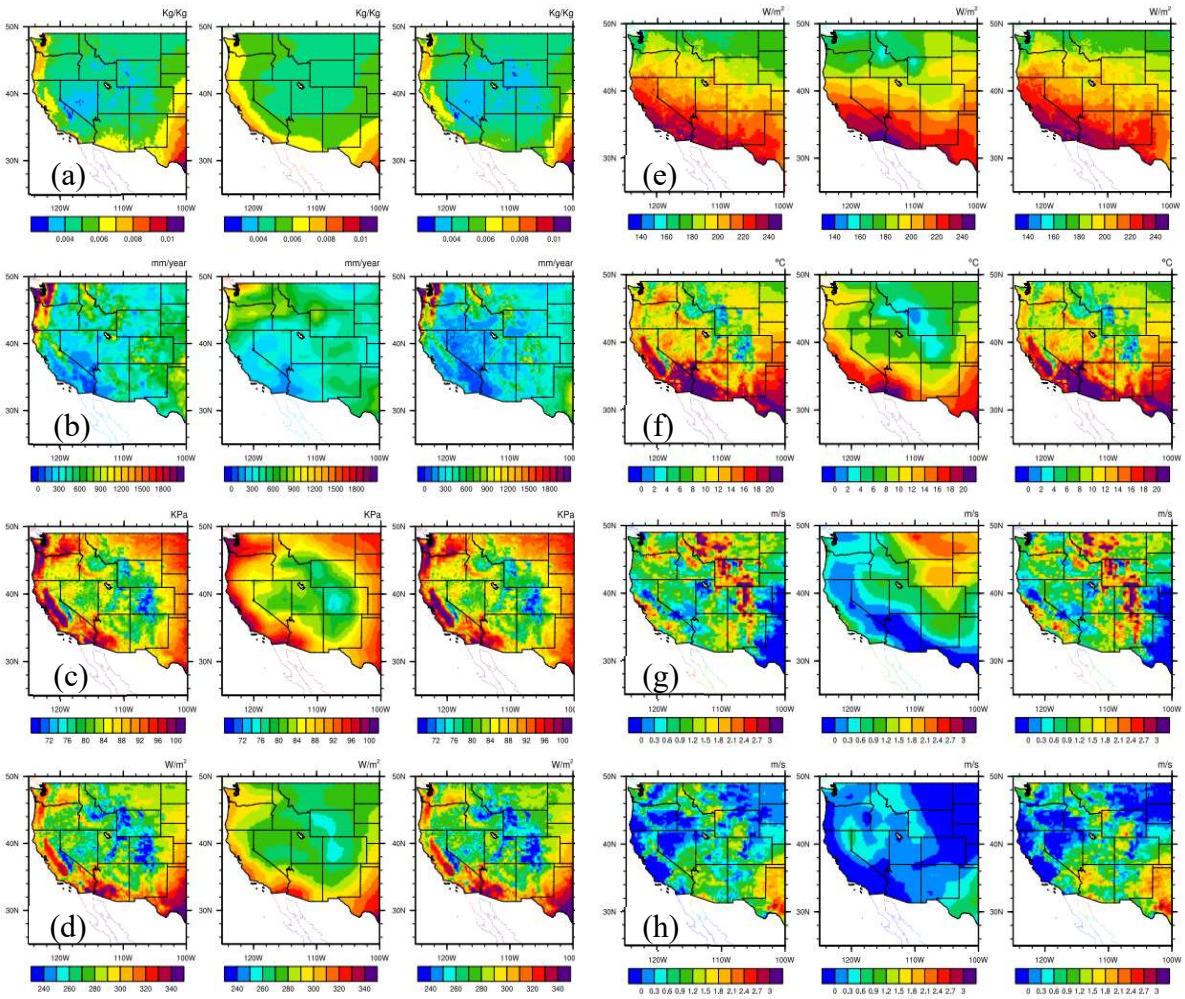

FIG. A1. Annual (a) specific humidity, (b) total precipitation, (c) surface air pressure, (d) downward longwave radiation, (e) downward shortwave radiation, (f) air temperature at 2 m, (g) zonal wind speed at 2 m, and (h) vertical wind speed at 2 m during 2015 of (left) observations, (center) original IPSL-CM5A-MR (RCP 8.5), and (right) downscaled IPSL-CM5A-MR (RCP 8.5).

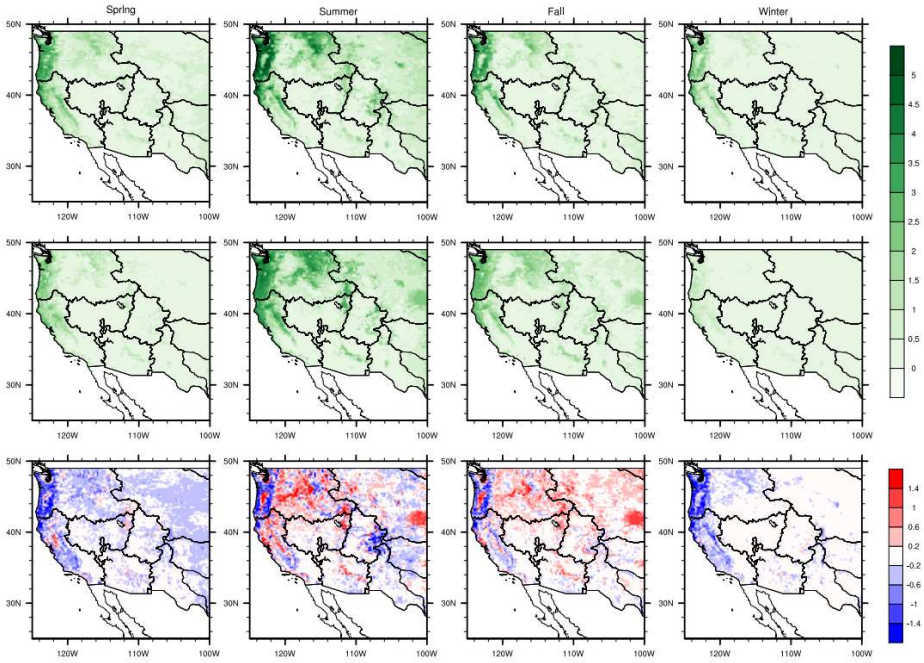

FIG. A2. Seasonal mean LAI from 2002 through 2015 of (top) MODIS, (middle) Noah-MP, and (bottom) Noah-MP minus MODIS (unit: m^2/m^2).

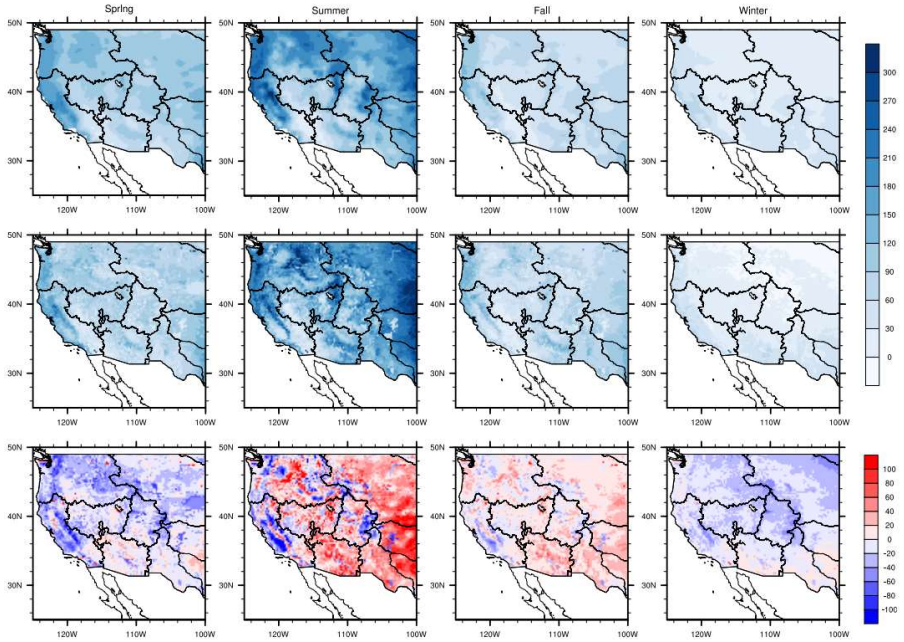

FIG. A3. Seasonal total ET from 1982 through 2011 of (a) FLUXNET-MTE; (b) Noah-MP, and (c) Noah-MP minus FLUXNET-MTE (unit: mm).

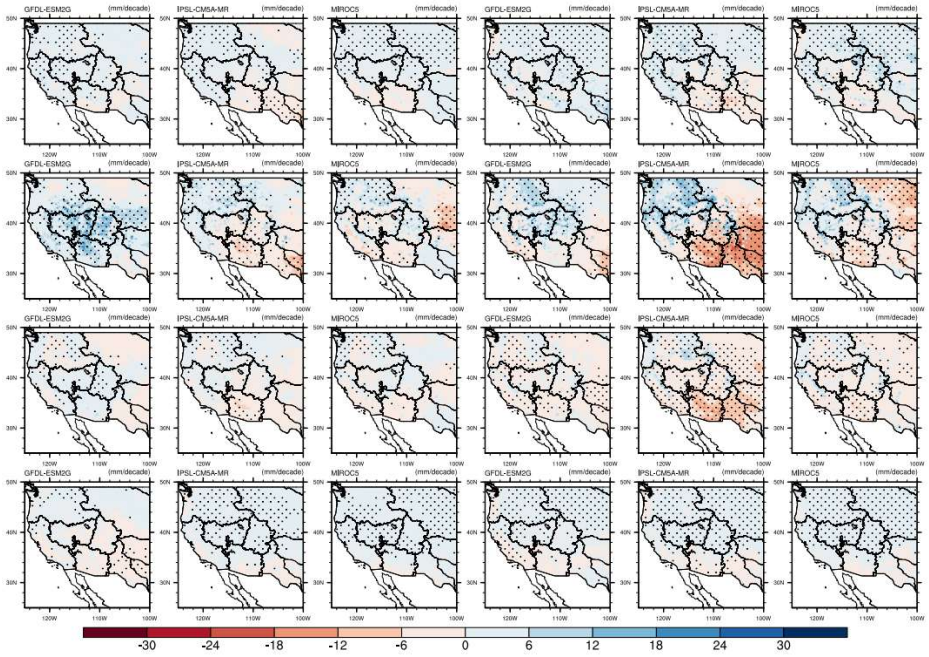

FIG. A4. Spatial distribution of trends in (a) spring, (b) summer, (c) fall, and (d) winter total evapotranspiration during 2016–2099 (unit: mm/decade) under RCPs 4.5 (left three columns) and 8.5 (right three columns). Stippling indicates regions with statistically significant trends ($p < 0.05$).

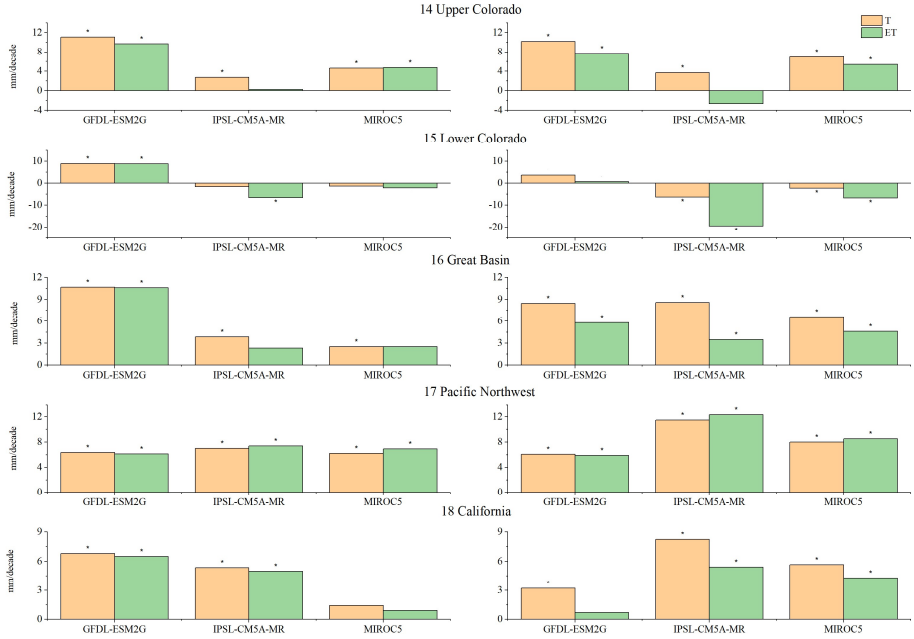

FIG. A5. Trends of annual total transpiration (T) and ET during 2016–2099 (unit: mm/decade). The asterisk indicates significant trends ($p < 0.05$).

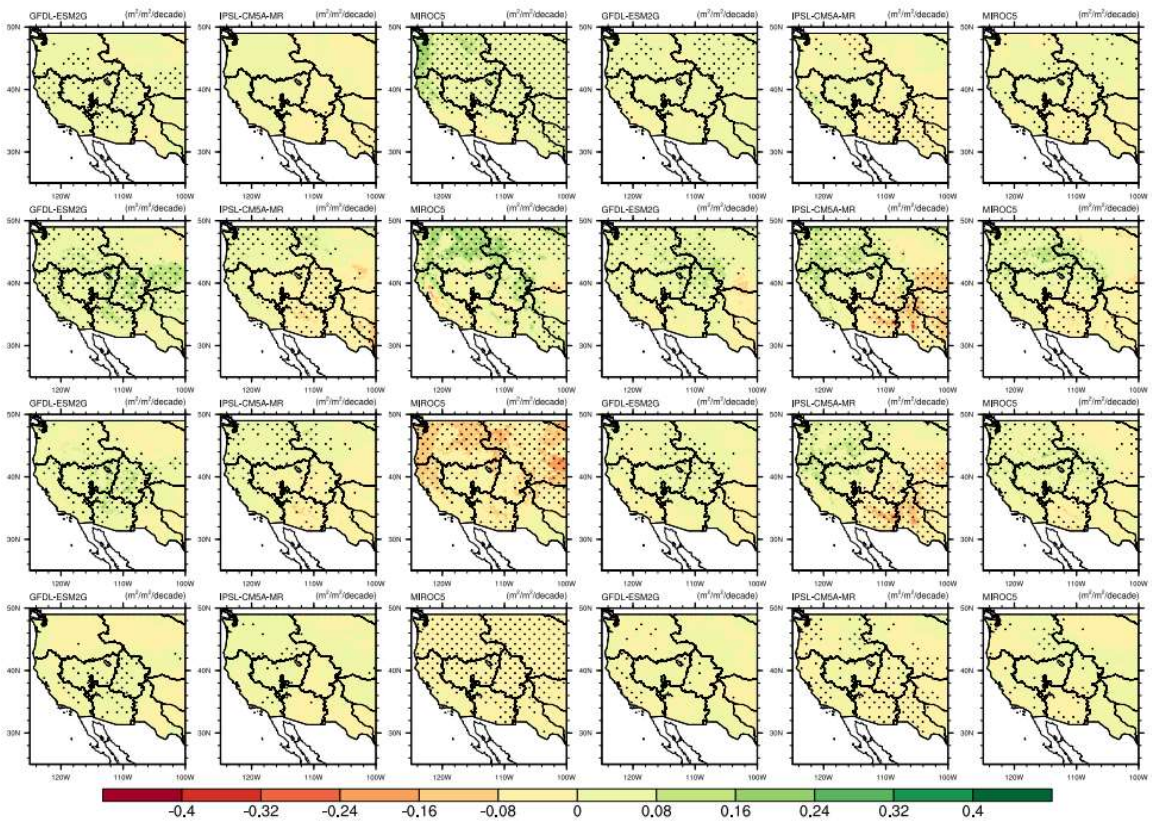

FIG. A6. Spatial distribution of trends in (a) spring, (b) summer, (c) fall, and (d) winter mean LAI during 2016–2099 (unit: m2/m2/decade) of the additional experiment under RCPs 4.5 (left three columns) and 8.5 (right three columns). Stippling indicates regions with statistically significant trends ($p < 0.05$).

TABLE A1. Seasonal and annual mean LAI trends averaged over regions 14–18 (unit: m^2/m^2/decade). Significant trends are shown in bold ($p < 0.05$).

Scenario		RCP 4.5			RCP 8.5		
Model		GFDL-ESM2G	IPSL-CM5A-MR	MIROC5	GFDL-ESM2G	IPSL-CM5A-MR	MIROC5
Region 14	Spring	**0.02**	**0.01**	**0.02**	**0.06**	**0.04**	**0.06**
	Summer	**0.15**	**0.04**	**0.06**	**0.21**	**0.09**	**0.15**
	Fall	**0.08**	**0.02**	**0.03**	**0.08**	0.01	**0.06**
	Winter	**0.01**	0	**0**	**0.01**	**0**	**0.01**
	Annual	**0.06**	**0.02**	**0.03**	**0.09**	**0.04**	**0.07**
Region 15	Spring	**0.03**	**0.02**	0.01	**0.10**	**0.04**	**0.05**
	Summer	**0.08**	0	0	**0.06**	-0.01	0.01
	Fall	**0.06**	-0.02	-0.01	0.03	**-0.07**	-0.01
	Winter	**0.01**	0	0	**0.02**	-0.01	0.01
	Annual	**0.05**	0	0	**0.05**	-0.01	0.02
Region 16	Spring	**0.02**	**0.02**	**0.01**	**0.06**	**0.07**	**0.05**
	Summer	**0.12**	**0.04**	**0.03**	**0.18**	**0.14**	**0.12**
	Fall	**0.06**	**0.02**	**0.01**	**0.03**	0	**0.02**
	Winter	0	**0**	**0**	0	0	0
	Annual	**0.05**	**0.02**	**0.02**	**0.07**	**0.05**	**0.05**
Region 17	Spring	**0.04**	**0.04**	**0.05**	**0.10**	**0.13**	**0.12**
	Summer	**0.10**	**0.09**	**0.08**	**0.18**	**0.18**	**0.18**
	Fall	**0.03**	**0.04**	**0.03**	**0.05**	**0.07**	**0.06**
	Winter	**0.01**	**0.01**	**0.01**	**0.01**	**0.02**	**0.02**
	Annual	**0.05**	**0.05**	**0.04**	**0.08**	**0.10**	**0.09**
Region 18	Spring	**0.07**	**0.05**	**0.03**	**0.12**	**0.15**	**0.12**
	Summer	**0.07**	**0.05**	**0.02**	**0.09**	**0.11**	**0.10**
	Fall	**0.03**	**0.03**	**0.01**	**0.03**	**0.03**	**0.04**
	Winter	**0.01**	**0.01**	**0**	0.02	**0.03**	**0.03**
	Annual	**0.04**	**0.04**	**0.02**	**0.06**	**0.08**	**0.07**

TABLE A2. Seasonal and annual total transpiration trends averaged over regions 14–18 (unit: mm/decade). Significant trends are shown in bold ($p < 0.05$).

Scenario		RCP 4.5			RCP 8.5		
Model		GFDL-ESM2G	IPSL-CM5A-MR	MIROC5	GFDL-ESM2G	IPSL-CM5A-MR	MIROC5
Region 14	Spring	**1**	**1**	**1**	**3**	**1**	**3**
	Summer	**8**	**2**	**3**	**6**	**3**	**4**
	Fall	**2**	0	**1**	**1**	**-1**	**1**
	Winter	0	0	0	0	0	**0**
	Annual	**11**	**3**	**5**	**10**	**4**	**7**
Region 15	Spring	**2**	**1**	0	**4**	1	**2**
	Summer	**5**	-1	-1	0	**-3**	**-2**
	Fall	**2**	**-2**	-1	-1	**-4**	**-2**
	Winter	**0**	0	0	0	**0**	0
	Annual	**9**	-2	-1	4	**-6**	**-2**
Region 16	Spring	**1**	**1**	**1**	**2**	**3**	**2**
	Summer	**8**	**2**	**1**	**7**	**7**	**4**
	Fall	**2**	1	0	0	-1	0
	Winter	0	0	0	0	0	0
	Annual	**11**	**4**	**3**	**9**	**9**	**7**
Region 17	Spring	**2**	**1**	**2**	**2**	**3**	**3**
	Summer	**4**	**5**	**4**	**5**	**8**	**5**
	Fall	1	**1**	**1**	**-1**	**1**	0
	Winter	**0**	0	0	0	0	0
	Annual	**6**	**7**	**6**	**6**	**11**	**8**
Region 18	Spring	**3**	**2**	**1**	**3**	**4**	**4**
	Summer	**4**	**3**	0	1	**4**	**2**
	Fall	1	1	0	**-1**	0	0
	Winter	**0**	0	0	**0**	0	0
	Annual	**7**	**5**	1	**3**	**8**	**6**

TABLE A3. Seasonal and annual total precipitation trends averaged over regions 14–18 (unit: mm/decade). Significant trends are shown in bold ($p < 0.05$).

Scenario		RCP 4.5			RCP 8.5		
Model		GFDL-ESM2G	IPSL-CM5A-MR	MIROC5	GFDL-ESM2G	IPSL-CM5A-MR	MIROC5
Region 14	Spring	**4**	-2	1	2	**-3**	1
	Summer	**6**	-3	1	3	**-10**	0
	Fall	**4**	-2	0	1	**-8**	-2
	Winter	-1	0	2	1	2	-1
	Annual	14	-7	4	8	**-18**	-2
Region 15	Spring	-1	-2	-1	-2	**-2**	-2
	Summer	**8**	**-7**	-2	2	**-14**	**-4**
	Fall	1	-2	0	0	**-9**	-2
	Winter	-1	0	-2	-1	-2	-2
	Annual	**7**	-10	-4	-1	**-26**	**-10**
Region 16	Spring	**5**	0	0	0	-1	-3
	Summer	**3**	0	1	2	-4	2
	Fall	2	0	-1	0	**-3**	0
	Winter	-2	2	0	0	2	1
	Annual	8	2	0	2	-6	-1
Region 17	Spring	4	1	1	**8**	1	3
	Summer	0	-2	-2	-4	0	-1
	Fall	-2	5	-1	-3	3	1
	Winter	-3	**8**	4	3	-2	5
	Annual	0	12	2	4	1	9
Region 18	Spring	4	2	-2	-4	-1	-3
	Summer	**2**	0	-1	-1	-2	1
	Fall	3	3	-5	**-8**	-2	2
	Winter	-7	11	-3	-5	-2	2
	Annual	3	15	-11	-16	-7	1

TABLE A4. Seasonal mean solar radiation trends averaged over regions 14–18 (unit: W/m^2/decade). Significant trends are shown in bold ($p < 0.05$).

Scenario		RCP 4.5			RCP 8.5		
Model		GFDL-ESM2G	IPSL-CM5A-MR	MIROC5	GFDL-ESM2G	IPSL-CM5A-MR	MIROC5
Region 14	Spring	**-1**	0	0	**-1**	**1**	**-1**
	Summer	**0**	0	0	0	0	**-1**
	Fall	**0**	0	0	0	**1**	0
Region 15	Spring	0	0	0	**1**	0	0
	Summer	**-1**	0	0	**0**	0	**0**
	Fall	0	0	0	0	**1**	0
Region 16	Spring	**-1**	0	0	**-1**	1	0
	Summer	**-1**	0	0	**-1**	0	**-1**
	Fall	0	0	0	0	**0**	0
Region 17	Spring	0	1	0	**-2**	1	0
	Summer	0	**0**	0	0	0	0
	Fall	0	0	0	0	0	0
Region 18	Spring	0	0	1	0	0	0
	Summer	**-1**	0	0	**-1**	**-1**	**-1**
	Fall	0	0	0	0	0	0

```
;The NCL code for interpolating low-resolution CMIP5 to high-resolution (~12 km) data, written by Xueyan Zhang
;Attention please: this script produces data with longitude in an order like (0,360), not (-180,-180)
;for specific humidity
begin

;cmip5 future data
  dirin = "/home/2017060321/zqh/data/CMIP5/downscaled/GFDL-ESM2G/rcp26/huss/fur/"
  diroutt = "/home/2014011989/Data/downscaling/GFDL-ESM2G/rcp26/huss/fur_us_0125/"
;observations providing lat and lon
  diriny  = "/home/2014011989/serial_JJM/Noah_data/static/"
  filiny  = "lon_lat.nc"

  stry  = 1979
  endy  = 2100
  do year = stry,endy

    filin     = "huss_3hr_GFDL-ESM2G_rcp26_r1i1p1_"  + year +  ".nc"
    filoutt   = "zqh_huss_GFDL-ESM2G_rcp26_" + year + ".nc"

    finy = addfile(diriny + filiny,"r")
    fin  = addfile(dirin+filin,"r")

    lat = finy->lat
    lon = finy->lon
    lon = 360.0+lon

    lon!0           = "lon"
    lon@long_name     = "longitude"
    lon@units         = "degrees_east"
    lon&lon           = lon
    lat!0           = "lat"
    lat@long_name     = "latitude"
    lat@units         = "degrees_north"
    lat&lat           = lat

    huss              = fin->huss

    tim       = fin->time
    dimn              = dimsizes(tim)-2
    k3        = ispan(0,(dimn+1)*125,125)
    time              = k3/1000.
```

```
ntimes   = dimsizes(time)
nrow     = dimsizes(lat)
ncol     = dimsizes(lon)

huss2    = linint2_Wrap(huss&lon,huss&lat,huss,False,lon,lat,0)
printMinMax(huss2, 1)

twhuss       = new((/ntimes,nrow,ncol/),float,"No_FillValue")
twhuss       = (/huss2/)
time!0       = "time"
time&time    :=time
twhuss!0     = "time"
twhuss!1     = "lat"
twhuss!2     = "lon"
twhuss&time  :=  time
twhuss&lat   =  lat
twhuss&lon   :=  lon-360.0
twhuss@_FillValue    = 1.e+20
twhuss@missing_value = 1.e+20
twhuss@units     = "kg kg-1"
twhuss@long_name  = "Near surface air specific humidity"

dimNames  =  (/"time","lat","lon"/)
dimSizes  =  (/ntimes,nrow,ncol/)
dimUnlim  =  (/False,False,False/)

system("rm -f "+diroutt+filoutt)
foutt= addfile(diroutt+filoutt,"c")
setfileoption(foutt,"DefineMode",True)

filedimdef(foutt,dimNames,dimSizes,dimUnlim)
foutt->lat  = lat
foutt->lon  = lon
foutt->huss = twhuss

delete(fin)
delete(foutt)
delete(twhuss)
delete(time)
delete(ntimes)
delete(k3)
delete(tim)
delete(lat)
delete(lon)
delete(huss)
delete(huss2)
```

```
    delete(finy)

  end do
end
```

###The bias-correction code for CMIP5 data were written by the FORTRAN code (Jiming Jin).

###Makefile

```
OBJS = scaler_main.o scaler.o sort.o qsort.o fit.o
NETCDF=/home/2015051066/soft/netcdf
FC=mpiifort
###FC=mpif90
FFLAG = -O3 -traceback -g -assume byterecl -heap-arrays 64 -mcmodel=medium -
DNETCDF4_HDF5 -DNETCDF4_COMPRESS
####FFLAG = -O2 -mcmodel=medium
scaler: $(OBJS)
	$(FC) -o $@ $(FFLAG) $(OBJS) -L$(NETCDF)/lib -lnetcdf -lnetcdff
scaler_main.o: scaler_main.F90
	$(FC) -c $(FFLAG) -I$(NETCDF)/include scaler_main.F90
scaler.o: scaler.F90
	$(FC) -c $(FFLAG) -I$(NETCDF)/include scaler.F90
sort.o: sort.F90
	$(FC) -c $(FFLAG) sort.F90
qsort.o: qsort.F90
	$(FC) -c $(FFLAG) qsort.F90
fit.o: fit.F90
	$(FC) -c $(FFLAG) fit.F90
clean:
	rm $(OBJS) scaler
```

```
!!!! scaler_main.F90
      implicit none
      include 'netcdf.inc'
      include 'mpif.h'
      integer nlat,nlon,nall,nyear,ntime
      integer :: mlon,mlat,ntime1!jjr

      parameter(nlat=224, nlon =464,ntime=2920)  !xyr
      parameter(nall=121,nyear=38)               !xyr
!jjr change mlon to 128,mlat to 256
      parameter(mlon=464,mlat=224,ntime1=1)!ntime1 can >1,if the cash is big
enough  !xyr

      character*25 name
      character*15 unit
      character*256 nf,ng
      character*256 fname
      character*256 cmd
      character*256 toutf(nall)

      real tccsm(mlon,mlat,nall,ntime1)
!jjr      real tccsm(mlon,mlat,lev,nall,ntime)
      real tncep(mlon,mlat,nyear,ntime1)
!jjr      real tncep(mlon,mlat,lev,nyear,ntime)
      real tn(mlon,mlat,ntime1),tc(mlon,mlat,ntime1)
!jjr      real tn(mlon,mlat,lev,ntime),tc(mlon,mlat,lev,ntime)

      integer timid,latid,lonid,ncid
      integer tim_id,lat_id,lon_id,var_id

      integer count(3),start(3)
      integer vardims(3)
      integer status,cdfid,varid,i,j,ip,jp,k,ik,ix,jx
      integer kn,kc,ka,iyear,it,ky,ic,ir,iv,imm

      real xlat(nlat),xlon(nlon),time(ntime)
      real dt(mlon,mlat,nall,ntime1), dtt(mlon,mlat,ntime1)
      real missv
      logical filefound
!jjr
      integer myproc,ierr,nproc,ntime2,ntime3,im,np1,np2
      integer endyear,ntime33,nt,kyy,iyy
!---------------------------------------------------------------
      call MPI_init(ierr)
      call MPI_Comm_Size(MPI_COMM_WORLD,nproc,ierr)
       call MPI_COMM_RANK(MPI_COMM_WORLD,myproc,ierr)
```

```
      np1=mod(ntime,nproc)
      np2=ntime/nproc
!jjr if mod(ntime,nproc).ne.0,ntime1 should =1
      if(myproc.lt.np1) then
       ntime2=np2+1
       ntime33=(np2+1)*myproc
      else
       ntime2=np2
       ntime33=(np2+1)*np1+np2*(myproc-np1)
      end if

      ky = 0
      do iyear=1980,2100  !xyr
       ky = ky + 1
       write(toutf(ky),7001) iyear
7001    format('/home/2014011989/Data/downscaling/GFDL-
ESM2G/rcp26/huss/reg/reg_huss_GFDL-ESM2G_rcp26_',i4,&
        '.nc')   !xyr
!       print*, toutf(ky),myproc
      end do

!jjr here nproc=146
!      ntime2=ntime/(nproc*ntime1) ! warning jjr,if mod(ntime,nproc*ntime1).ne.0) ,it
need rewrite
      missv = -999.9   !xyr

      iyear = 1980     !xyr
      write(fname,555) iyear
555   format('/home/2014011989/Data/downscaling/GFDL-
ESM2G/rcp26/huss/fur_us_0125/huss_GFDL-ESM2G_rcp26_',&
       i4,'.nc')   !xyr
      if(myproc.eq.0)       print*,fname

      status = nf_open(trim(fname),nf_nowrite,cdfid)
      if (status .ne. nf_noerr) call handle_err(status)
      status = nf_inq_varid(cdfid,'lat',varid)
      status = nf_get_vara_real(cdfid,varid,1,nlat,xlat)
      if (status .ne. nf_noerr) call handle_err(status)
      status = nf_inq_varid(cdfid,'lon',varid)
      status = nf_get_vara_real(cdfid,varid,1,nlon,xlon)
      if (status .ne. nf_noerr) call handle_err(status)
      status = nf_close(cdfid)

!-----------------------------------------------
      ky = 0
!here can rewrite divide iyear to severeal processors
```

```
       np1=mod(121,nproc)  !xyr
       np2=121/nproc
      if(myproc.lt.np1) then
       nt=np2+1
       kyy=(np2+1)*myproc
      else
       nt=np2
       kyy=(np2+1)*np1+np2*(myproc-np1)
      end if
       if(nt.ge.1) then
!      do iyear=1948,2099
       do iyy=1,nt
        iyear=kyy+1980+iyy-1    !xyr
         ky=kyy+iyy

!       ky = ky + 1
       write(toutf(ky),700) iyear
700    format('/home/2014011989/Data/downscaling/GFDL-
ESM2G/rcp26/huss/reg/reg_huss_GFDL-ESM2G_rcp26_',i4,&
       '.nc')  !xyr
!       print*, toutf(ky)

       inquire (file=trim(toutf(ky)), exist=filefound)
       if (filefound) then
         write (cmd, 666)  trim(toutf(ky))
666        format('/bin/rm -f ',a)
         call system (trim(cmd))
       endif
       status = nf_create(toutf(ky), nf_noclobber, ncid)
       if (status .ne. nf_noerr) call handle_err(status)

       status = nf_def_dim(ncid, 'time',nf_unlimited, timid)
       if (status .ne. nf_noerr) call handle_err(status)
       status = nf_def_dim(ncid, 'lat', nlat, latid)
       if (status .ne. nf_noerr) call handle_err(status)
       status = nf_def_dim(ncid, 'lon', nlon, lonid)
       if (status .ne. nf_noerr) call handle_err(status)

       name = 'since 1-1-1 00:00:00'
       unit = '3 hours'   !xyr
       status = nf_def_var(ncid,'time',nf_float,1,timid,tim_id)
       if (status .ne. nf_noerr) call handle_err(status)
       status = nf_put_att_text(ncid,tim_id,'long_name',len(name),&
        name)
       if (status .ne. nf_noerr) call handle_err(status)
       status = nf_put_att_text(ncid,tim_id,'units' ,len(unit), &
```

```
 unit)
 if (status .ne. nf_noerr) call handle_err(status)

 name = 'latitude'
 unit = 'degrees_north'
 status = nf_def_var(ncid,'lat', nf_float,1,latid,lat_id)
 if (status .ne. nf_noerr) call handle_err(status)
 status = nf_put_att_text(ncid,lat_id,'long_name',len(name),&
 name)
 if (status .ne. nf_noerr) call handle_err(status)
 status = nf_put_att_text(ncid,lat_id,'units' ,len(unit),&
 unit)
 if (status .ne. nf_noerr) call handle_err(status)

 name = 'longitude'
 unit = 'degrees_east'
 status = nf_def_var(ncid,'lon', nf_float,1,lonid,lon_id)
 if (status .ne. nf_noerr) call handle_err(status)
 status = nf_put_att_text(ncid,lon_id,'long_name',len(name),&
  name)
 if (status .ne. nf_noerr) call handle_err(status)
 status = nf_put_att_text(ncid,lon_id,'units' ,len(unit),&
  unit)
 if (status .ne. nf_noerr) call handle_err(status)

 vardims(1) = lonid
 vardims(2) = latid
 vardims(3) = timid

name   = 'Near surface air specific humidity'   !xyr
unit   = 'kg kg-1'                              !xyr
status = nf_def_var(ncid,'huss',nf_float,3,vardims,var_id)
 if (status .ne. nf_noerr) call handle_err(status)
status = nf_put_att_text(ncid,var_id,'long_name',len(name),&
  name )
 if (status .ne. nf_noerr) call handle_err(status)
status = nf_put_att_text(ncid,var_id,'units' ,len(unit),&
 unit)
 if (status .ne. nf_noerr) call handle_err(status)
status = nf_put_att_real(ncid,var_id,'missing_value',&
 nf_float, 1,  missv)
 if (status .ne. nf_noerr) call handle_err(status)
 status = nf_close(ncid)

 do imm=1,2920
   time(imm) = iyear*100+ imm
```

```
      end do

      status = nf_open(toutf(ky),nf_write,ncid)
      if (status .ne. nf_noerr) call handle_err(status)
      status=nf_put_vara_real(ncid,tim_id,1,ntime,time)
      if (status .ne. nf_noerr) call handle_err(status)
      status=nf_put_vara_real(ncid,lat_id,1,nlat,xlat)
      if (status .ne. nf_noerr) call handle_err(status)
      status=nf_put_vara_real(ncid,lon_id,1,nlon,xlon)
      if (status .ne. nf_noerr) call handle_err(status)
      status = nf_close(ncid)
     end do
      endif
!jjr use first cpu to write/read file information
!jjr move ntimes to the outer do loops

!-----------------------------------------------
     call MPI_BARRIER(MPI_COMM_WORLD,ierr)
     if(ntime2.ge.1) then
     do im=1,ntime2 !jjr
       ntime3=ntime33+im ! the real time
!jjr begin test part if im.eq.ntime2,the mpp run finished
!         print*,'test mpp calculate',im,ntime3,myproc
!end end test part
      print*,'test' , im

      if(im.eq.ntime2) print*,'test1'
!     do ic=1,nlon,mlon
!     do ir=1,nlat,mlat
!     kn = 0 !kn is useless
     if(myproc.lt.121) then  !xyr
     kc = myproc !jjr iyear=1948+myproc ---> kc=myproc
     kn=myproc
!warning if 1948+myproc>2099,it should be rewrite
!jjr the processor myproc read/write file(year) from 1948+myproc to 2099,and from
1948to 1948+myproc-1
     do iyear =1980+myproc,2100  !xyr
     write(nf,100) iyear
100   format('/home/2014011989/Data/downscaling/observations/yl/NLDAS_',&
      i4,'.nc')   !xyr

     write(ng,200) iyear
200   format('/home/2014011989/Data/downscaling/GFDL-
ESM2G/rcp26/huss/fur_us_0125/huss_GFDL-ESM2G_rcp26_',&
      i4,'.nc')
!     start(1) = ic
```

```
      start(1) = 1
      start(2) = 1
!     start(2) = ir
!     start(4) = 1
      start(3) = ntime3  !jjr

      count(1) = mlon
      count(2) = mlat
      count(3) = ntime1
!     count(4) = ntime

      if(iyear.le.2017) then   !xyr

        status = nf_open(nf,nf_nowrite,cdfid)
        status = nf_inq_varid(cdfid,'huss',varid)
        if (status .ne. nf_noerr) call handle_err(status)
        status = nf_get_vara_real(cdfid,varid,start,count,tn)
        if (status .ne. nf_noerr) call handle_err(status)
        status = nf_close(cdfid)
        kn = kn + 1
        tncep(:,:,kn,:) = tn
      end if

      status = nf_open(ng,nf_nowrite,cdfid)

      status = nf_inq_varid(cdfid,'huss',varid)
      if (status .ne. nf_noerr) call handle_err(status)
      status = nf_get_vara_real(cdfid,varid,start,count,tc)
      if (status .ne. nf_noerr) call handle_err(status)
      status = nf_close(cdfid)
      kc = kc + 1
      tccsm(:,:,kc,:) = tc

      end do ! iyear
      end if
      if(myproc.ne.0) then
        endyear=1980+myproc-1  !xyr
        if(myproc.ge.121) endyear=2100   !xyr
        kc=0!jjr iyear=1948 --->kc=0
        kn=0
      do iyear =1980,endyear   !xyr
      write(nf,1001) iyear
1001   format('/home/2014011989/Data/downscaling/observations/yl/NLDAS_',&i4,'.nc')
      write(ng,2001) iyear
2001   format('/home/2014011989/Data/downscaling/GFDL-
ESM2G/rcp26/huss/fur_us_0125/huss_GFDL-ESM2G_rcp26_',&i4,'.nc')
```

```
!jjr      start(1) = ic
      start(1) = 1
!jjr      start(2) = ir
      start(2) = 1
!      start(4) = 1
      start(3) = ntime3   !jjr

      count(1) = mlon
      count(2) = mlat
      count(3) = ntime1
!      count(4) = ntime

      if(iyear.le.2017) then    !xyr

        status = nf_open(nf,nf_nowrite,cdfid)
        status = nf_inq_varid(cdfid,'huss',varid)
        if (status .ne. nf_noerr) call handle_err(status)
        status = nf_get_vara_real(cdfid,varid,start,count,tn)
        if (status .ne. nf_noerr) call handle_err(status)
        status = nf_close(cdfid)
        kn = kn + 1
        tncep(:,:,kn,:) = tn
      end if

      status = nf_open(ng,nf_nowrite,cdfid)

      status = nf_inq_varid(cdfid,'huss',varid)
      if (status .ne. nf_noerr) call handle_err(status)
      status = nf_get_vara_real(cdfid,varid,start,count,tc)
      if (status .ne. nf_noerr) call handle_err(status)
      status = nf_close(cdfid)
      kc = kc + 1
      tccsm(:,:,kc,:) = tc
      end do !iyear
      end if

      call scaler(tncep,tccsm,nyear,nall,dt,mlon,mlat)
       if(myproc.eq.0)  print*,'end scaler,begin out',im
      if(myproc.lt.121) then   !xyr
      ky = myproc
      do iyear=1980+myproc,2100
      ky = ky + 1
      dtt = dt(:,:,ky,:)
      status=nf_open(trim(toutf(ky)), nf_write, ncid)
      if (status .ne. nf_noerr) call handle_err(status)
      status = nf_inq_varid (ncid, 'huss', var_id)
```

```
      if (status .ne. nf_noerr) call handle_err(status)

!jjr      start(1) = ic
      start(1) = 1
!jjr      start(2) = ir
      start(2) = 1
      start(3) = 1
!      start(4) = 1
      start(3) = ntime3
      count(1) = mlon
      count(2) = mlat
      count(3) = ntime1
!      count(4) = ntime

      status=nf_put_vara_real(ncid,var_id,start,count,dtt)
      if (status .ne. nf_noerr) call handle_err(status)
      status= nf_close(ncid)

      end do !iyear
      end if
      if(myproc.ne.0) then
          endyear=1980+myproc-1
        if(myproc.gt.121) endyear=2100
        ky=0
      do iyear=1980,2100
      ky = ky + 1
      dtt = dt(:,:,ky,:)
      status=nf_open(trim(toutf(ky)), nf_write, ncid)
      if (status .ne. nf_noerr) call handle_err(status)
      status = nf_inq_varid (ncid, 'huss', var_id)
      if (status .ne. nf_noerr) call handle_err(status)

!     start(1) = ic
      start(1) = 1
!     start(2) = ir
      start(2) = 1
!     start(4) = 1
      start(3) = ntime3
      count(1) = mlon
      count(2) = mlat
      count(3) = ntime1
!     count(4) = ntime

      status=nf_put_vara_real(ncid,var_id,start,count,dtt)
      if (status .ne. nf_noerr) call handle_err(status)
      status= nf_close(ncid)
```

```
      end do !iyear
      end if

!      end do
!      end do
      end do  !im
      end if
!-----------------------------------------------------------------
       call mpi_finalize(ierr)
      stop
      end

      subroutine handle_err(status)
        include 'netcdf.inc'
        integer status
        if (status .ne. nf_noerr) then
          print*, nf_strerror(status)
          stop 'Stopped'
        endif
      end
```

!!! scaler.F90

```
      subroutine scaler(tobs,tsim,nyear,nall,dt,mlon,mlat)
      implicit none
      integer ntime1
      parameter(ntime1=1)
      integer k,iy,im,nyear,nall
      integer mlon,mlat
      integer :: ic,ir
      real xa(ntime1),xb(ntime1),xrs(ntime1)
      real obst(nyear)
      real tobs(mlon,mlat,nyear,ntime1)

      real simt(nall)
      real tsim(mlon,mlat,nall,ntime1)

      real dt(mlon,mlat,nall,ntime1)
!-------------------------------------------------------------------------------

      do ic=1,mlon
      do ir=1,mlat

      do im=1,ntime1
        k=0
        do iy=1,nyear
           k=k+1
           simt(k)=tsim(ic,ir,iy,im)
           obst(k)=tobs(ic,ir,iy,im)
        enddo   ! iy

!jjr      call sort(k,obst)
          call quicksort(obst,1,nyear)
!jjr      call sort(k,simt)
          call quicksort(simt,1,nyear)
          call fit(k,simt,obst,xa(im),xb(im),xrs(im))
      enddo    ! im

      do iy=1,nall
      do im=1,ntime1
         dt(ic,ir,iy,im) = xa(im)+xb(im)*tsim(ic,ir,iy,im)
      enddo   ! im
      enddo    ! iy

      enddo
      enddo
      return
      end
```

!! sort.F90

```
      subroutine sort(n,p)
      dimension p(1)
      do i=1,n-1
       do j=i+1,n
         if(p(i).gt.p(j)) then
          t=p(j)
          p(j)=p(i)
          p(i)=t
         endif
       enddo
      enddo
      return
      end
```

!! qsort.F90

```
recursive subroutine quicksort(item, s, t)
implicit none
real  item(1)
integer s, t
integer k
if(s .lt. t) then
call quickpass(item, s, t, k)
call quicksort(item, s, k - 1)
call quicksort(item, k + 1, t)
endif
end
subroutine quickpass(item, s, t, k)
implicit none
real item(1)
integer s, t
integer k
real pivot
integer i, j
pivot = item(s)
i=s
j=t
do while(i .lt. j)
do while(i .lt. j .and. item(j) .ge. pivot)
j = j - 1
enddo
item(i) = item(j)
do while(i .lt. j .and. item(i) .le. pivot)
i = i + 1
enddo
item(j) = item(i)
```

```
enddo
item(i) = pivot
k = i
end
```

!!fit.F90

```
      subroutine fit(nl,odd,pdo,alpha,beta,ss)
      real pdo(1),odd(1)
      real mx,my

      mx=0.
      my=0.
      sx=0.
      sy=0.
      c=0.

      do i=1,nl
        mx=mx+odd(i)
!jjr       mx=mx+odd(i)/nl
        my=my+pdo(i)
!jjr       my=my+pdo(i)/nl
        sx=sx+odd(i)*odd(i)
!jjr       sx=sx+odd(i)*odd(i)/nl
        sy=sy+pdo(i)*pdo(i)
!jjr       sy=sy+pdo(i)*pdo(i)/nl
        c=c+odd(i)*pdo(i)
!jjr       c=c+odd(i)*pdo(i)/nl
      enddo
       mx=mx/nl
       my=my/nl
       sx=sx/nl
       sy=sy/nl
       c=c/nl
      sx=sqrt(sx-mx*mx)
      sy=sqrt(sy-my*my)
      c=(c-mx*my)/sx/sy
      beta=c*sy/sx
      alpha=my-beta*mx
      ss=c*c

      return
      end
```